Molecular Therapy
Oncology
Original Article

Non-viral TcBuster transposon engineering of CD70-CAR natural killer cells for the treatment of osteosarcoma

Gabrielle M. Robbins,[1,2,3,4] Jae-Woong Chang,[1,3,4] Joshua B. Krueger,[1,3,4] Young Y. Vue,[1,3,4] Alexandria K. Gilkey,[1,3,4] Timothy D. Folsom,[1,3,4] Tyler Jubenville,[1,3] Joseph G. Skeate,[1,3,4] Benjamin W. Langworthy,[5,6] Katelyn M. Fitzgerald,[1] Joseph J. Peterson,[1,3,4] Erin M. Stelljes,[1,3,4] David A. Largaespada,[1,3,7] Eric P. Rahrmann,[8,9] Beau R. Webber,[1,3,4,10] and Branden S. Moriarity[1,3,4,10]

[1]Department of Pediatrics, University of Minnesota, Minneapolis, MN, USA; [2]College of Veterinary Medicine, University of Minnesota, Minneapolis, MN, USA; [3]Masonic Cancer Center, University of Minnesota, Minneapolis, MN, USA; [4]Center for Genome Engineering, University of Minnesota, Minneapolis, MN, USA; [5]School of Public Health, University of Minnesota, Minneapolis, MN, USA; [6]Clinical and Translational Science Institute, University of Minnesota, Minneapolis, MN, USA; [7]Department of Genetics, Cell Biology and Development, University of Minnesota, Minneapolis, MN, USA; [8]Cancer Research UK Cambridge Institute, University of Cambridge, Cambridge, UK; [9]Hormel Institute, University of Minnesota, Austin, MN, USA

Osteosarcoma (OSA) is the most common primary bone tumor in children and adolescents, yet outcomes have remained largely unchanged for over 40 years. While chimeric antigen receptor (CAR) T cell therapy has shown success in blood cancers, it faces major limitations in solid tumors due to immune evasion, antigen loss, and immunosuppressive tumor microenvironments. Natural killer (NK) cells offer several advantages over T cells, including multiple killing mechanisms and lower risks of graft-versus-host disease, neurotoxicity, and cytokine release syndrome, making them promising candidates for off-the-shelf cell therapies. However, unmodified NK cells have shown limited efficacy in clinical settings due to poor engraftment, persistence, and tumor-mediated suppression. To overcome these barriers, we developed a cost-effective method to engineer CAR NK cells targeting CD70, a tumor antigen overexpressed in relapsed and metastatic OSA. We further enhanced these cells by incorporating soluble interleukin-15 (IL-15) and a dominant-negative TGF-β receptor, creating "armored" CAR NK cells. These engineered cells resist transforming growth factor β (TGF-β) suppression, secrete IL-15, and demonstrate improved cytotoxicity, persistence, and tumor homing in both *in vitro* and *in vivo* models. Our findings support CD70 CAR NK cells as a promising immunotherapeutic strategy for relapsed and metastatic OSA.

INTRODUCTION

Osteosarcoma (OSA) is the most common primary malignancy of bone diagnosed in children and adolescents with approximately 900 newly diagnosed cases annually in the United States.[1] Although the 5-year survival rate of OSA patients with localized disease is over 70%, this rate drops below 30% if there are any clinically apparent metastases.[2,3] Nearly one-third of OSA patients have overt metastases at diagnosis and another 40% will develop lung metastases later during the course of disease.[3–5] These data highlight that metastasis is a common occurrence and the top factor associated with poor patient outcomes in OSA.[6] Despite advances in our understanding of OSA biology, treatment options have not changed significantly over the last four decades and continue to focus on tumor resection and combination chemotherapy.[7] Currently, immunotherapeutic approaches have shown promise with other cancer types but remain relatively unexplored for OSA.[8]

Natural killer (NK) cells are lymphocytes of the innate immune system that can recognize and kill virally infected and transformed cells without prior sensitization in a non-human leukocyte antigen (HLA)-restricted manner.[9] NK cells play a critical role in the elimination of tumor cells, prevention of tumor cell metastases, and immune surveillance.[10] NK cells are activated upon interaction with tumor cells through ligands found on tumor cells. Once activated, NK cells can directly release granzymes and perforin, mediate antibody-dependent cellular cytotoxicity (ADCC) via their CD16A receptor, or activate apoptotic pathways mediated by Fas ligand (FasL) or tumor necrosis factor (TNF)-related apoptosis-inducing ligand (TRAIL).[11,12] In addition to these direct methods of killing target cells, NK cells produce cytokines and chemokines such as interferon gamma (IFN-γ) and TNF-α, which can activate adaptive immunity and/or result in target cell necrosis or apoptosis.[13] Additionally, NK cells can be effectively equipped to target specific tumor antigens through the installation of a chimeric antigen receptor (CAR). CARs are engineered receptors designed to graft immune effector cells with

Received 11 September 2025; accepted 11 December 2025;
https://doi.org/10.1016/j.omton.2025.201119.

[10]These authors contributed equally

Correspondence: Branden Moriarity, Department of Pediatrics, University of Minnesota, Minneapolis, MN, USA.
E-mail: mori0164@umn.edu

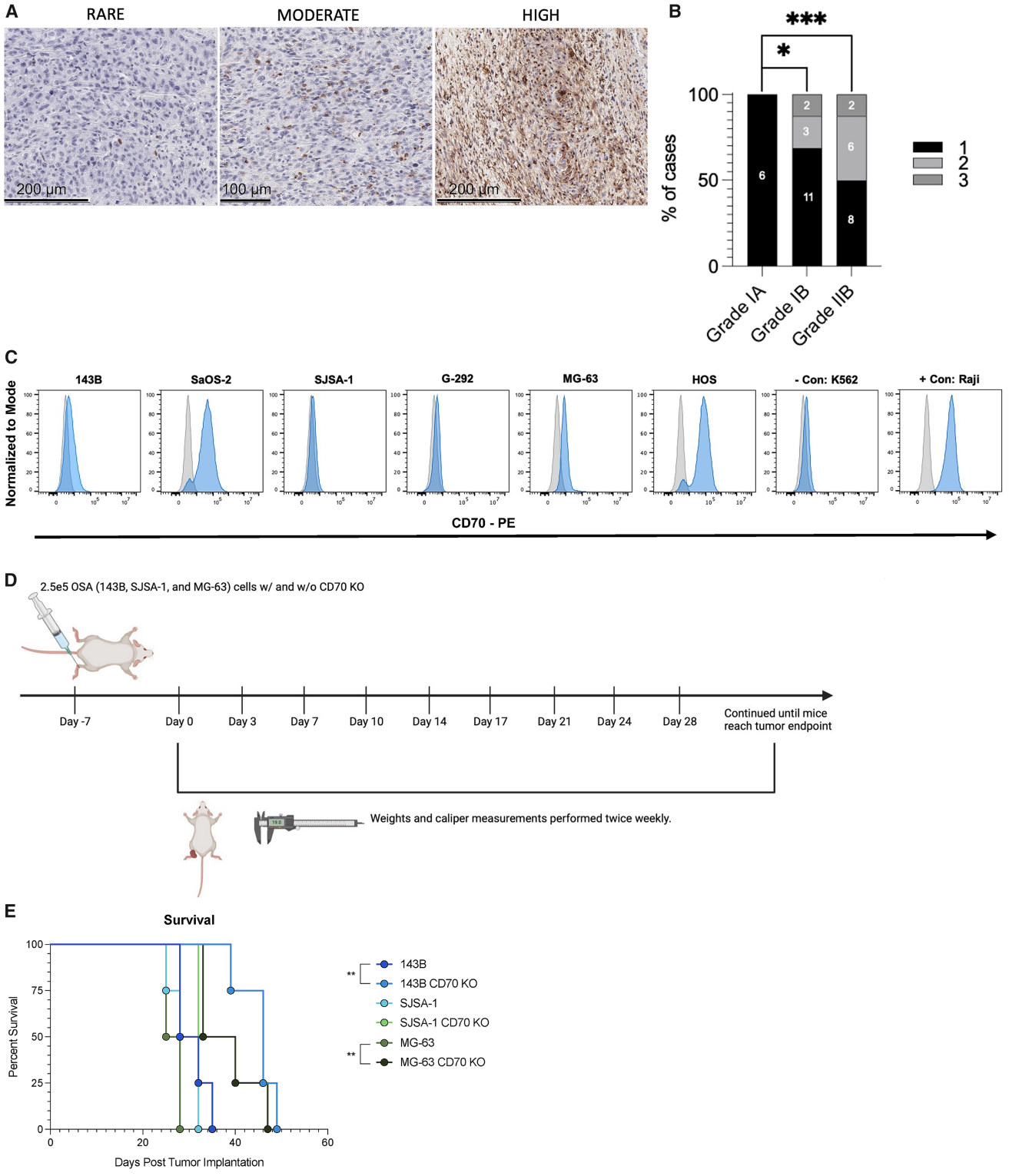

Figure 1. CD70 expression is increased in high-grade and metastatic osteosarcoma

(A) Representative score images for histological evaluation of OSA tissue microarray containing two samples each for 40 patients (n = 80). The scale bar for each image is 200 μm. (B) Bar graph comparison of scores for OSA tissue microarray samples by tumor grade. Fisher's exact test performed showed IA vs. IB FET p = 0.0130, IA vs. IIB FET

(legend continued on next page)

the ability to specifically target tumor-associated antigens (TAAs), independent of MHC presentation, and activate modified cells through signal transduction.[14] Historically, most studies have evaluated CARs in T cells for the treatment of various cancers. CAR-T cell therapies have been successful in the treatment of hematological cancers, which has sparked interest into designing new CARs for the treatment of more diverse malignancies, including solid tumors.[15]

When compared to T cells, NK cells present several advantages as an immunotherapy. While CAR-T cells have shown success in the treatment of hematologic malignancies, they have been associated with several drawbacks, such as high manufacturing costs and substantial toxicities in the form of cytokine release syndrome (CRS) and immune-effector-cell-associated neurotoxicity syndrome (ICANS).[14,16,17] NK cells make for attractive effector cells for CAR engineering because of their cytokine profile, which differs from those produced by T cells.[18] NK cells do not carry the risk of graft-versus-host disease (GvHD) and as such, have the potential to be an off-the-shelf cellular product available for immediate clinical use.[19] In immunologically cold tumors, like OSA, CAR-NK cells have an advantage over CAR-T cells, as NK cells exhibit rapid cytotoxicity that is not major histocompatibility complex (MHC)-dependent, show less exhaustion, and are able to be activated through a variety of innate signaling pathways beyond TAAs.[20] Conversely, CAR-T cells and other immunotherapeutics are limited in instances of antigen escape, whereas NK cells are naturally equipped with several cytotoxicity pathways that can still be activated in the absence of CAR TAA expression.

CD70 is a member of the TNF family that upon binding its receptor, CD27, regulates the survival and activation of T, B, and NK cells.[21] It has also emerged as a promising target that is actively being investigated as a CAR target in several tumor types, including acute myeloid leukemia (AML), glioblastoma, T cell lymphomas, and renal cell carcinoma (RCC).[22–26] In normal tissue, CD70 is transiently expressed by activated antigen-presenting cells (APCs), T cells, and NK cells.[27] Similarly, CD70 has not been detected on normal hematopoietic stem cells (HSCs), suggesting that targeting CD70 would not adversely affect hematopoiesis.[22] The minimal expression of CD70 on normal, healthy tissues alongside supports the notion that targeting of CD70 expressing tumors will have limited off-tumor effects. In fact, several CD70-targeted therapies are currently in clinical trials, including CD70 CAR-T cells (NCT05420519, NCT02830724, NCT05468190, and NCT04662294), CD70-specific antibodies (NCT01677390 and NCT04227847), and bispecific T cell engagers (BiTEs) (NCT05673057). Together, these studies have demonstrated a high level of safety. A CD70-CAR-NK-cell-based therapy provides an alternative treatment that is more cost effective with potential as a safer, more effective, off-the-shelf therapy.

Although NK cells are potent effector cells, tumor cells develop mechanisms to evade NK cell recognition and/or suppress NK cell function.[28] Some of these evasion modalities include, but are not limited to, upregulating expression of MHC class 1 molecules and producing immunosuppressive cytokines (e.g., interleukin (IL)-10 or transforming growth factor β [TGF-β])].[29] One method of engineering NK cells to overcome tumor evasion of NK cell recognition is through the introduction of a CAR.

Here, we report an efficient and effective approach to generate CD70 CAR NK cells using the *TcBuster* transposon system in combination with Cas9-mediated knockout (KO) of endogenous CD70. Transposons provide a non-viral engineering strategy to introduce several transgenes in a single vector that can be scaled effectively for clinical use. Further, our engineering strategy enhances NK activity and antitumor function through the inclusion of a secreted supportive cytokine (IL-15) and a TGF-β dominant-negative mutant receptor (DNR). We evaluated these armored CD70 CAR NK cells against OSA cell lines *in vitro* for killing capacity, cytokine production, activation, and exhaustion after target cell challenge. Finally, we tested these CD70 CAR NK cells *in vivo* against orthotopic and intravenous mouse xenograft models. Our work provides critical preclinical data for the use of CD70 CAR NK cells for the treatment of primary and metastatic OSA.

RESULTS

CD70 expression in osteosarcoma varies by stage of disease and CD70 knockout improves xenograft survival

CD70 has recently emerged as an actionable immunotherapy target and has shown potential for OSA.[23,30–32] To determine the promise of a CD70-targeted therapy for OSA, we performed immunohistochemical (IHC) analysis of CD70 on an OSA tissue microarray (TMA) with 40 unique patient primary tumor samples (Creative Bioarray). The IHC staining results were assigned a mean score based on the intensity of the staining. Samples with absent or very low levels of CD70 staining were assigned a score of 1, samples with moderate staining a score of 2, and samples with high immunoreactivity to CD70 were assigned a score of 3. Representative IHC images for each score, 1–3, are shown in Figure 1A. As there were two samples for each patient, the average of the patient was used, and a Fisher's exact test was performed. The results from the IHC scoring showed that 32.5% of samples ($n = 13$) had moderate (2) to high (3) staining, and there was a statistically significant incidence ($p = 0.0003$) of increased CD70 staining in higher-grade osteosarcoma (Figure 1B).

$p = 0.0003$, and IB vs. IIB FET p = ns ($\alpha = 0.05$, $^{*}p < 0.05$, $^{**}p < 0.01$, $^{***}p < 0.001$, $^{****}p < 0.0001$). (C) Evaluation of CD70 expression in several osteosarcoma cell lines by flow cytometry. K562 is included as a negative control and Raji as a positive control. (D) NSG mice were injected intraosseously with 2.5E5 OS cells (143B, SJSA-1, and MG-63) with or without CD70 knockout. Shown is schematic of study timeline, including OSA cell implantation into NSG mice ($n = 4$/cell line) as well as weight and caliper measurements. Primary tumors were harvested at endpoint (tumor volume = 1 cm^3) as well as lungs. Tumors and lungs were fixed and paraffin embedded. (E) Kaplan-Meier survival curve of mice injected intraosseously with OS cells with or without CD70 KO ($n = 4$). Survival significance was determined by a Log rank (Mantel-Cox) test between groups.

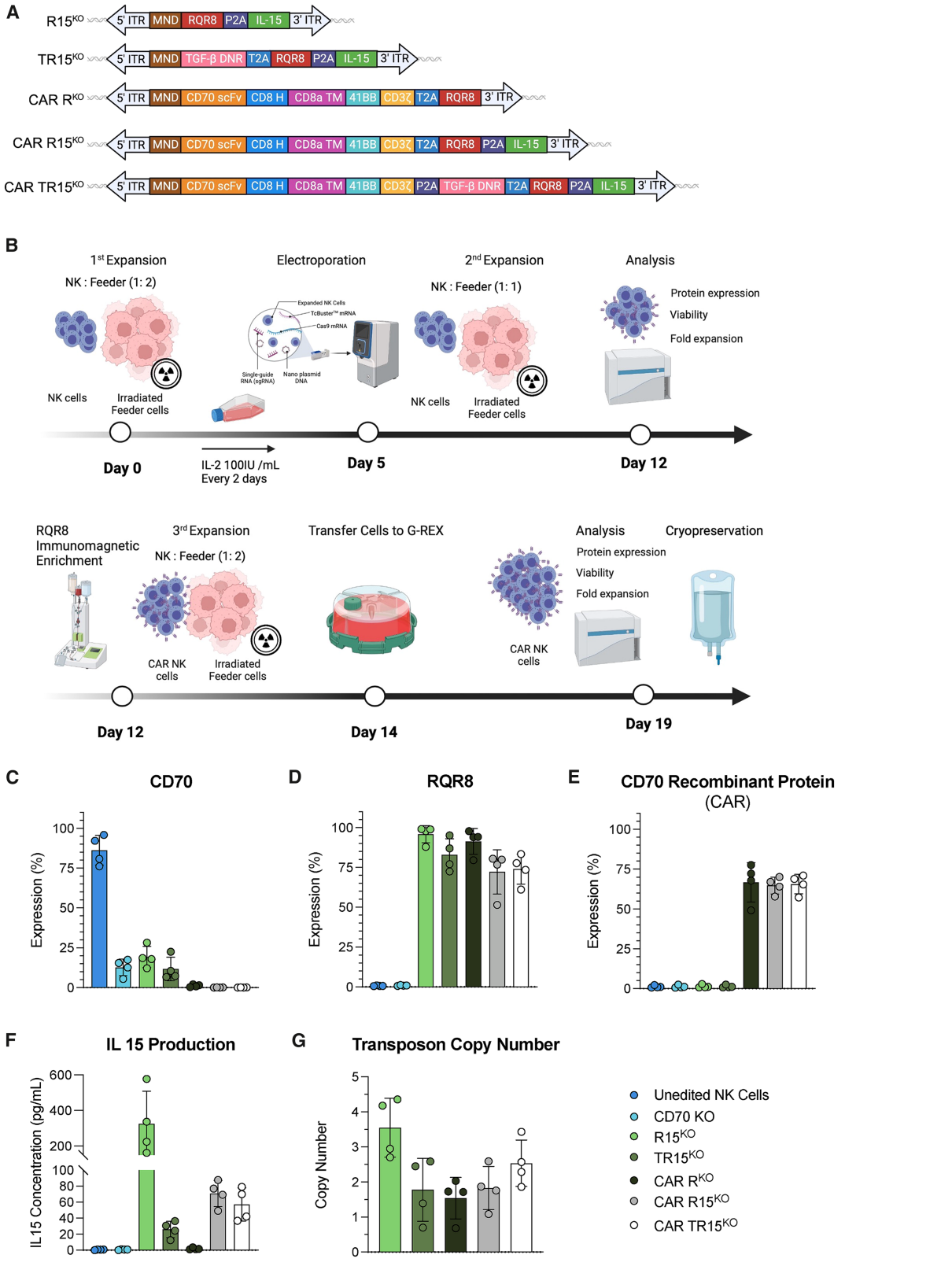

(legend on next page)

Our data are in line with previous reports of CD70 expression in OSA.[30,31] Additionally, we analyzed six osteosarcoma cell lines for CD70 expression using flow cytometry (Figure 1C). SJSA-1 and G-292 were negative for CD70. 143B and MG-63 had moderate levels of CD70 (19.7% and 33.8% of cells were positive for CD70). HOS and SaOS-2 had the greatest percentage of cells expressing CD70 at 92.2% and 90.5%, respectively.

CD70 expression in OSA has been linked to recurrent and/or metastatic samples.[30,31] As metastatic spread is the primary factor associated with poor patient outcome, we wanted to further investigate the relationship between CD70 expression and recurrent and/or metastatic disease in OSA. To this end, OSA cell lines with varying levels of CD70 expression (143B, MG-63, and SJSA-1) were implanted intraosseously (2.5E5 cells) into the calcaneal bone of 6-week-old NSG mice. These mice were sacrificed at tumor endpoint (tumor volume of 1 cm^3), and primary tumors, lungs, and livers were harvested. After tissues were fixed and decalcified, samples were paraffin embedded, sectioned, and stained for CD70 and human mitochondria. Interestingly, IHC showed diffuse CD70 staining of endpoint primary tumors and metastatic lung lesions despite none of these cell lines showing high CD70 expression *in vitro* (Figure 1D). This study was followed by the generation of CD70 KO lines for 143B, MG-63, and SJSA-1. In parallel to the WT OSA cell lines, these CD70 KO cell lines were implanted intraosseously (2.5E5 cells) into the calcaneal bone of 6-week-old NSG mice. Kaplan-Meier survival curve showed for 143B ($p = 0.0062$) and MG-63 ($p = 0.0084$), CD70 KO significantly increased survival. These data demonstrate that high CD70 expression in OSA correlates with aggressive disease features, while CD70 knockout significantly improves survival in mice, highlighting its potential as a therapeutic target.

Efficient engineering of CD70 CAR NK cells using TcBuster transposition and CRISPR/Cas9

Given our IHC findings showing increased CD70 expression in lung metastases of xenograft mouse models, CD70 is a potentially key target for relapsed and metastatic OSA. The upregulation of CD70 in endpoint primary tumors and lung metastases in our initial IHC findings indicate CD70 has the potential for targeted therapy for advanced OSA patients (Figure 1D). We thus designed several different transposon constructs to engineer healthy-donor-derived peripheral blood NK cells (Figure 2A). Our CD70 CAR contains a CD70 single-chain variable fragment (scFv), CD8 hinge, CD8α transmembrane domain, 4-1BB costimulatory domain, and CD3ζ signaling domain. Our fully armored construct also contains a TGF-β DNR, RQR8, and soluble IL-15 (Table S1). TGF-β is known to be highly prevalent in the OSA tumor microenvironment, favoring growth of the primary tumor and the dissemination of metastases.[33,34] By including a TGF-β DNR in our constructs, we aimed to functionally inactivate TGF-β signaling in NK cells, rendering them unresponsive to TGF-β-mediated immunosuppression.[35] RQR8 is a combination of epitopes from both CD34 and CD20 antigens that serves as a combination marker to indirectly assess engineering efficiency and serve as a suicide gene via use of rituximab.[36] Finally, we included soluble IL-15 in our transposon expression cassettes to allow NK cells to secrete IL-15, promoting *in vivo* survival, proliferation, and persistence.[37] In our transposon constructs, we utilized the MND synthetic promoter, which can be widely introduced into both dividing and nondividing cells and is highly active in lymphohematopoietic cells.[38]

Fratricide is common in NK cells and represents intentional negative feedback regulation, often mediated through trogocytosis.[39] Following initial challenges in engineering CD70 CAR NK cells (data not shown), CRISPR/Cas9-mediated knockout proved to be critical to prevent fratricide post-engineering and was done in every condition except for the unedited NK cells. Thus, we expanded NK cells from healthy, de-identified donors by co-culture with irradiated K562 feeder cells expressing membrane bound IL21 (mbIL21) and 41BBL[40] for 5 days before electroporating them with transposon plasmid and mRNA encoding *TcBuster* transposase with or without mRNA encoding Cas9 and chemically modified synthetic guide RNA-targeted CD70 using the MaxCyte electroporation system (Figure 2B). The seven NK cell conditions used throughout this study include unedited NK cells, CD70 KO NK control, RQR8-IL15 with CD70 KO ($R15^{KO}$), TGF-β DNR RQR8-IL15 with CD70 KO ($TR15^{KO}$), CD70 CAR RQR8 with CD70 KO (CAR R^{KO}), CD70 CAR RQR8-IL15 with CD70 KO (CAR $R15^{KO}$), and CD70 CAR TGF-β DNR RQR8-IL15 with CD70 KO (CAR $TR15^{KO}$).

NK cells were expanded immediately following electroporation at a 1:1 ratio using irradiated feeder cells. After 7 days, cells were analyzed via flow cytometry for CD70, RQR8, and CAR expression using CD70 recombinant protein (Figures 2C–2E). CD70 knockout averaged >85%; however, in CAR NK cell conditions, NK cells without successful knockout were eliminated, likely due to fratricide (Figure 2C).[39] Knockout efficiency, indel distribution, and off-target editing were assessed at the genomic level (Figure S1). CRISPR/Cas9 off-target analysis was performed using one sample from cells treated with CD70 sgRNA ("Sample") and one sample from unedited NK

Figure 2. Simultaneous delivery of CD70 CAR using the TcBuster transposon system and CRISPR/Cas9 knockout of *CD70* expanded to clinically relevant numbers within 20 days

(A) Transposon constructs flanked by TcBuster inverted terminal repeats (ITRs), containing an MND promoter and various cargo, including CD70 CAR, RQR8, IL-15, and/or TGF-β dominant-negative mutant receptor (DNR). (B) Schematic of primary human peripheral blood (PB) NK cell ($n = 4$ healthy human donors) engineering timeline. (C–E) CD70, RQR8 (CD34), and CD70 recombinant protein expression in engineered NK cells assessed by flow cytometry. Bar graphs show the percentage of live cells positive for the indicated target; error bars show the standard deviation ($n = 4$ NK cell donors). (F) IL-15 production in pg/mL by engineered NK cells assessed by IL-15 ELISA. Values represent the average of three technical replicates performed for each donor ($n = 4$ NK cell donors); error bars show the standard deviation. (G) Results from construct insertion copy-number analysis determined by digital droplet PCR ($n = 4$ NK cell donors); error bars show the standard deviation.

cells ("Control" = NK cells electroporated with non-targeting reagents) (Figure S1). Results showed that of the 58 off-target sites, 4 had off-target editing at <1% relative to the control sample, suggesting the sgRNA chosen shows little off-target activity. CAR vector integration efficiency was assessed through RQR8 expression and CD70 recombinant protein binding (Figures 2D and 2E). RQR8 expression averaged >72% and CD70 recombinant protein binding >64%. NK cells incubated for 24 h in media only secreted between 0 and 577.5 μg/mL of IL-15, with RQR8-IL15 groups secreting the most at 161.7–577.5 μg/mL, as measured by ELISA (Figure 2F). Transposon copy numbers were assessed for each construct and found to be less than 4.5 copies for each transgene (Figure 2G). These data demonstrate that we can successfully use *TcBuster* and Cas9 engineering contemporaneously to generate CAR NK cells that show little Cas9 off-target editing with copy numbers within the Food and Drug Administration (FDA) guidelines (<5).[41] TcBuster integration and safety were evaluated at length in previously published work.[42]

Functional validation of CD70 CAR NK cells against osteosarcoma *in vitro*

CD70 CAR NKs and controls were evaluated in functional assays against the OSA cell lines 143B and SaOS-2. We selected these lines as they represent moderate (143B) and high (SaOS-2) CD70 expression. NK and CAR NK cells were co-cultured with luciferase expressing OSA cells for 48 h at various effector-to-target (E:T) ratios, adjusted for CAR-positivity. CAR TR15^{KO} NK cells showed superior killing compared to other conditions, particularly at the lowest E:Ts (Figure 3A). By 48 h, these fully armored CD70 CAR NK cells showed 100% killing at higher E:T ratios and nearly 50% killing of both 143B and SaOS-2 at the lowest E:T ratio of 1:32, specifically noting significant differences between TR15^{KO} NK and CAR TR15^{KO} NK (143B p = <0.0001, SaOS-2 p = 0.0053) (Figures 3B, S2, and S3).

To further assess levels of functional degranulation and cytokine production through intracellular cytokine staining, CAR NK and controls were co-cultured at a 1:1 E:T ratio against SaOS-2 and 143B. CD70 CAR NK cells cultured with SaOS-2 showed significantly more CD107a on their surface and produced greater quantities of IFN-γ and TNF-α than NK cells that did not express the CD70 CAR (Figure 3C). No statistically significant differences in cytokine staining were detected between NK cell conditions co-cultured against 143B (Figure S4). Heat maps from SaOS-2 co-cultures demonstrate that CAR-expressing NK cells produce significantly greater CD107a and TNF-α (Figure 3D). Taken together, these data demonstrate that CAR TR15^{KO} NK cells show significantly improved *in vitro* functional efficacy against SaOS-2 when compared to baseline CAR NKs.

In depth *in vitro* assessment of CD70 CAR NK cell cytokine and chemokine secretome

To further assess NK cells for potential in their cytokine/chemokine profiles due to engineering, supernatant was collected following co-culture experiments. This supernatant was analyzed by nELISA, a high-throughput protein profiling platform to assess 191 different cytokines and chemokines.[43] We tested for differences between effector cell conditions for each of the 191 cytokine and chemokine targets. Cytokines and chemokines with adjusted p values that showed a statistically significant difference at the assessed E:T ratios are highlighted in red (Figure 4A). Co-cultures against 143B only showed a statistically significant difference in IL-15 levels (p = 0.009). There was significantly more cytokine and chemokine activity against target cell line SaOS-2, including CCL1 (p = 0.014), CCL2 (p = 0.029), CCL7 (p = 0.018), CX3CL1 (0.009), CXCL10 (p = 0.003), CXCL11 (p = 0.013), CXCL9 (p = 0.001), granulocyte-macrophage colony-stimulating factor (GM-CSF) (p = 0.022), IFN-γ (p = 0.045), IL-15 (p = 0.024), matrix metalloproteinase 10 (MMP-10) (p = 0.03), MMP-9 (p = 0.003), TNF-α (p = 0.015), and vascular endothelial growth factor C (VEGF-C) (p = 0.003). Multiple comparisons showing cytokines and chemokines in co-culture experiments with target cell SaOS-2 at a 1:32 E:T ratio show CAR TR15^{KO} NK have dramatic difference in cytokine and chemokine activity compared to other NK cell conditions (Figure 4B). CAR TR15^{KO} NK cells show an increase in pro-inflammatory cytokines (IFN-γ, TNF-α, GM-CSF) as well as chemokines associated with adaptive cell recruitment (CXCL9, CXCL16, CCL3, and CX3CL1). These data suggest that CAR TR15^{KO} NK cells show potent cytotoxic activity and secrete cytokines capable of recruiting other immune effector cells to the TME. While we see similar trends in co-cultures against 143B, the changes in cytokine and chemokine activity are not as drastic as seen against SaOS-2. Additional comparisons were generated to show cytokines and chemokines elevated in different constructs. Comparisons of TR15^{KO} NK cells (positive) to CAR TR15^{KO} NK cells (negative) are shown at 1:32 E:T ratio against 143B and SaOS-2 (Figures 4C and 4D). These comparisons show dramatic differences in cytokine and chemokine activity between TR15^{KO} NK cells with and without a CD70 CAR, highlighting those identified in the heat maps. These data highlight that CAR TR15^{KO} NK cells are potent anti-tumor cells that release pro-inflammatory cytokines as well as chemokines necessary for the recruitment of other immune cell subsets. This may be highly advantageous against an immunologically cold tumor, like OSA.

In an effort to investigate potential advantages the cytokine profile may confer upon interaction with OSA tumors, ingenuity pathway analysis (IPA) of the nELISA dataset was carried out.[44,45] The analysis overall shows upregulation of inflammatory pathways with concurrent downregulation of immunosuppressive and tumorigenic pathways (Figure S6). Specifically, we found that there was an upregulation of canonical and non-canonical nuclear factor κB (NF-κB) pathways, which play a critical role in the immune response.[46] Similarly, the TNF family is shown to be upregulated and is critical in activating the host immune system and actively inducing apoptosis in cancerous cells.[47] Interestingly, there is also upregulation of macrophage classical activation signaling, which is involved in increasing phagocytosis, promoting secretion of pro-inflammatory cytokines (TNF-α, IL-1β, and

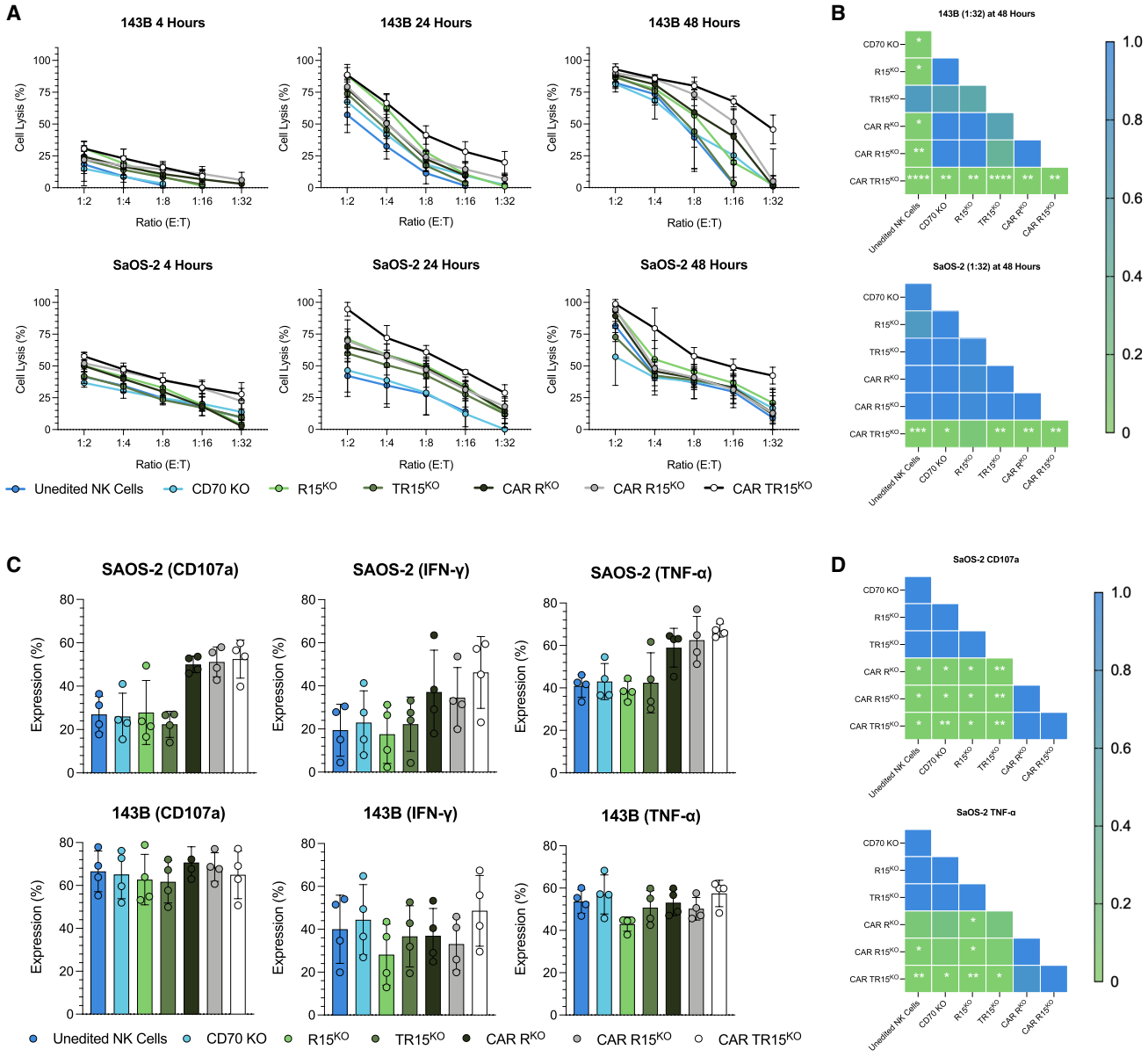

Figure 3. Armored CD70 CAR NK cells demonstrate robust *in vitro* killing of CD70+ osteosarcoma cell lines

(A) Engineered NK cells were co-cultured with luciferase-expressing OSA cell lines, 143B and SaOS-2, at the indicated E:T ratios for 4, 24, and 48 h. Each point represents the donor average (n = 4 NK cell donors), and the error bars show the standard deviation. Each condition (target cell, E:T, effector) was repeated in triplicate. (B) Co-culture experiments were analyzed using two-way ANOVAs with Tukey's multiple comparisons tests. p values from the Tukey's multiple comparisons were used to generate heat maps; heat maps for co-cultures against SaOS-2 and 143B at 48 h at a 1:32 E:T ratio are shown ($\alpha = 0.05$, $^{*}p < 0.05$, $^{**}p < 0.01$, $^{***}p < 0.001$, $^{****}p < 0.0001$). (C) Engineered NK cells were co-cultured with OSA cells, 143B and SaOS-2, at a 1:1 E:T ratio. Intracellular cytokine staining (ICS) was performed for CD107a, TNF-α, and IFN-γ in triplicate for each donor (n = 4 NK cell donors); error bars show standard deviation. (D) ICS results were analyzed using two-way ANOVAs with Tukey's multiple comparisons tests. p values from the Tukey's multiple comparisons were used to generate heat maps; heat maps for ICS against SaOS-2 for CD107a and TNF-α are shown ($\alpha = 0.05$, $^{*}p < 0.05$, $^{**}p < 0.01$, $^{***}p < 0.001$, $^{****}p < 0.0001$).

IL-6), and antigen presentation to T cells.[48] Upregulation of IL-17 indicates CAR TR15KO NK cells promote inflammation, support recruitment of other immune cells, and activate both CD8+ T cells and NK cells.[49] We also see downregulation of HEY1, which promotes tumor proliferation and inhibits apoptosis in cancers like OSA.[50] Similarly, we see downregulation of other pro-tumor signaling pathways, including the S100 family, tissue factor signaling, inhibitor differentiation 1 (ID1), HOTAIR, and

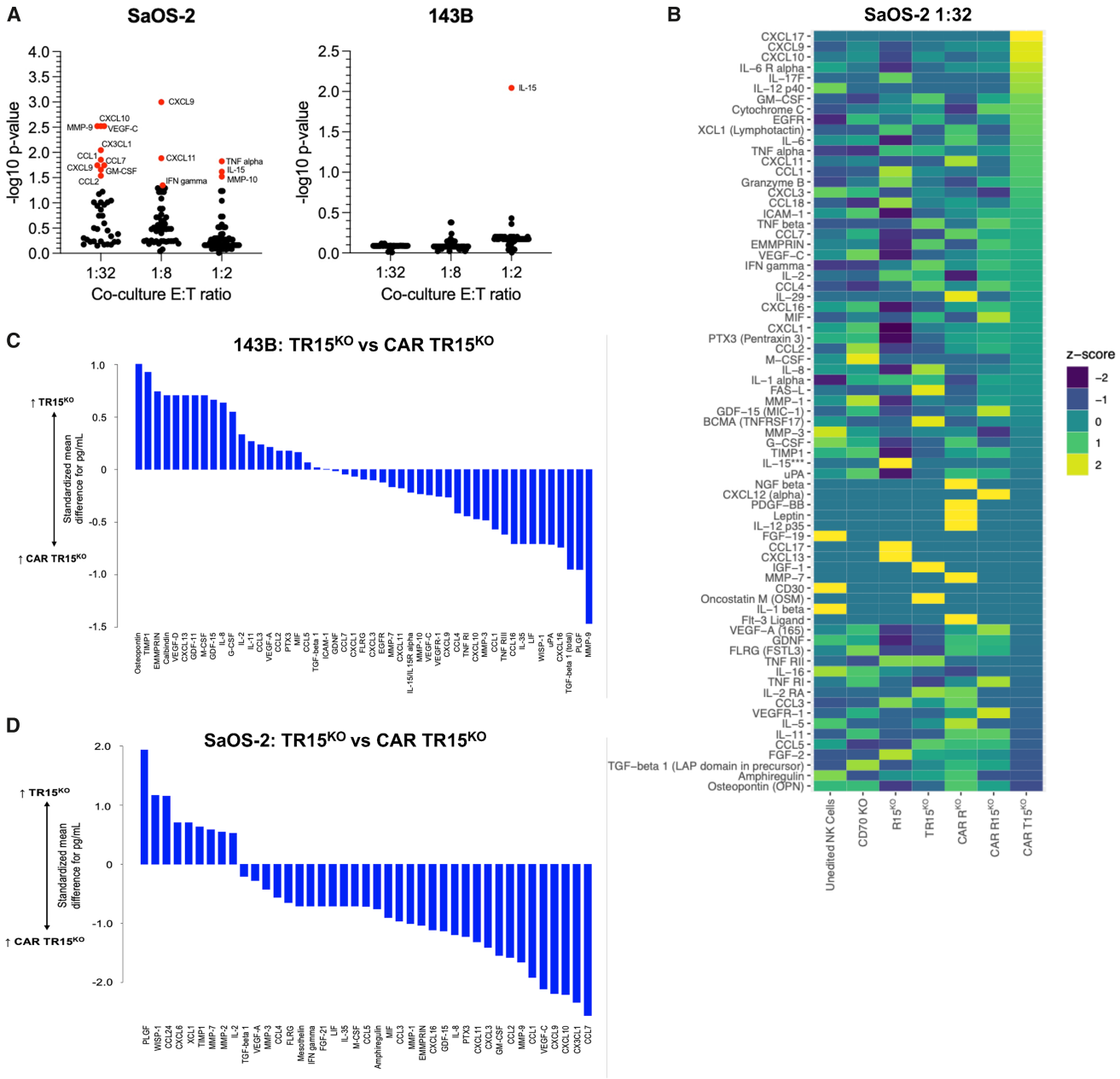

Figure 4. Computational modeling of cytokine and chemokine profiling of armored CD70 CAR NK cells shows a diverse landscape of anti-tumor responses

(A) Dot plot showing nELISA cytokines and chemokines with a significant difference between co-culture conditions, shown as -log(*p* value). One hundred ninety-nine (191) cytokines and chemokines were assessed by nELISA ($n = 4$ NK cell donors per E:T ratio). (B) Heat maps were generated showing *Z* scores for the different NK cell conditions, averaged by donor ($n = 4$) for the target cytokines/chemokines. The heatmap shown is for SaOS-2 at a 1:32 E:T ratio. (C and D) Waterfall plots comparing $TR15^{KO}$ (positive *y* axis) and CAR $TR15^{KO}$ (negative *y* axis) NK cells at a 1:32 E:T ratio with target cells 143B (C) and SaOS-2 (D). Values are standardized mean differences [(mean 1–mean 2)/sqrt(var1/2 + var 2/2)] ($n = 4$ NK cell donors).

the tumor microenvironment pathway. Together, these data suggest CAR $TR15^{KO}$ NK cells hold promise as an effective frontline therapy that allows us to target the primary tumor while potentially engaging the host immune system to prime *de novo* anti-tumor immunity.

Anti-tumor efficacy of CD70 CAR NK cells against an orthotopic mouse model of osteosarcoma

To test *in vivo* efficacy, we first injected $Luciferase^{+}/GFP^{+}$ 143B OSA cells intraosseously into the left calcaneal bone of NSG mice. Mice were randomized into eight groups 7 days post-tumor cell

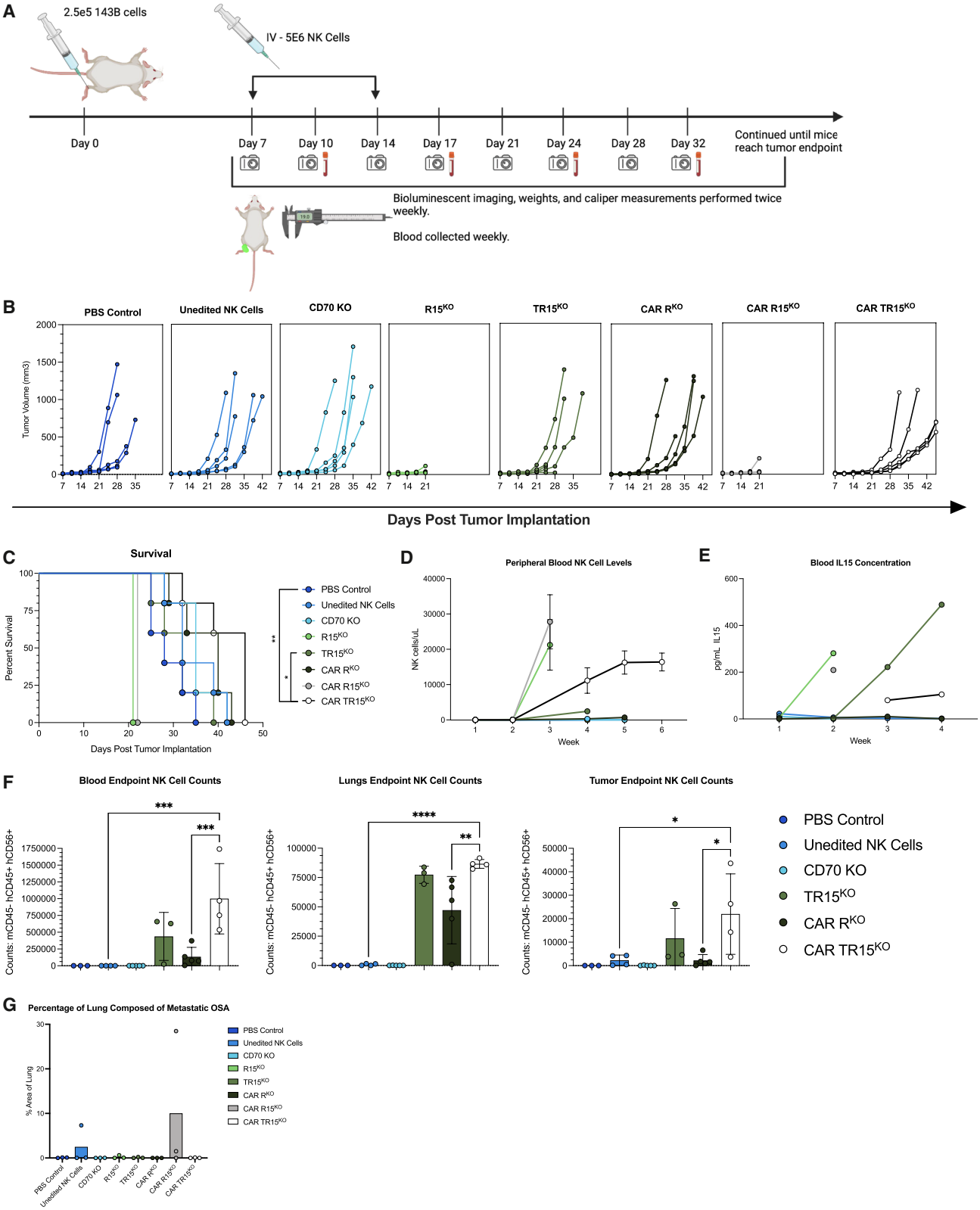

(legend on next page)

implantation. One of eight treatments (PBS control, unedited NK cells, CD70 KO, $R15^{KO}$, $TR15^{KO}$, CAR R^{KO}, CAR $R15^{KO}$, and CAR $TR15^{KO}$) were administered intravenously (i.v.) via tail vein injection on both 7 and 14 days post-tumor cell implantation (Figure 5A). Mice were assessed for general health, weighed, imaged using the IVIS Spectrum imaging system, and tumors measured twice weekly. A weekly blood sample was also collected. Due to variations in tumor growth rates and therapeutic response between animals, tumor volumes were reported using spaghetti plots (Figure 5B). Mice treated with CAR $TR15^{KO}$ NK cells survived the longest with three of five mice displaying a dramatic decrease in tumor growth rate (Figures 5B and 5C). Notably, by day 35, three mice treated with CAR $TR15^{KO}$ NK cells still had tumors <300 mm^3 (Figure 5B). Peripheral blood was assessed weekly for NK cells and IL-15 concentration (Figures 5D and 5E). CAR $TR15^{KO}$ NK cells showed sustained persistence in the blood and maintained IL-15 production. IL-15 production was significantly higher early in the study for $R15^{KO}$- and CAR-$R15^{KO}$-NK-cell-treated mice. These mice showed dramatic weight loss and were euthanized with suspected IL-15-related toxicity, as previously described by our group[51] and others.[52]

Once mice reached tumor endpoint, mice were euthanized and necropsies performed. Primary tumors, lungs, and liver were harvested, dissociated, and analyzed by flow cytometry for the presence of live NK cells. Blood from animals was also harvested and subjected to the same flow cytometric analysis. Tissues from CAR-$TR15^{KO}$-NK-cell-treated mice showed the greatest NK cell infiltration, particularly compared to unedited NK cells (blood $p = 0.0003$, lungs $p = <0.0001$, and tumor $p = 0.0357$) and non-armored CAR NK cells (CAR R^{KO}) (blood $p = 0.0009$, lungs $p = 0.0054$, and tumor $p = 0.0241$) (Figure 5F). Mice treated with $R15^{KO}$ and CAR $R15^{KO}$ NK cells did not have endpoint tissues analyzed, as these animals died prematurely due to suspected IL-15 toxicity. Tissues harvested at endpoint were fixed, decalcified, paraffin embedded, sectioned, and stained for CD70. Lungs were analyzed using QuPath to determine the total area of lung tissue composed of metastatic disease. These areas were graphed over total lung volume (Figure 5G). Coupled with the survival data, the lung tissue analysis suggests that most mice given control treatments reached primary tumor endpoint prior to the formation of lung metastases. Additionally, CAR-$TR15^{KO}$-NK-cell-treated mice survived longest and did not have any metastatic disease. Taken together, these data suggest that our fully armored CAR NK therapy can control tumors better than control NK conditions.

DISCUSSION

Cell-based immunotherapies have been a major focus for the treatment of cancer in recent decades.[53] Most research has focused on T-cell-based therapies, with NK cells and other immune cell populations only gaining favor within the last decade.[54] While several immunotherapies have shown preclinical promise against OSA specifically, this has not translated into clinical success. There are several factors limiting the efficacy of immunotherapies, specifically CAR therapies, against solid tumors; these include a lack of TAAs, failure of engineered cell homing to the tumor, lack of persistence, and an immunosuppressive tumor microenvironment.[55] Additionally, autologous CAR T cells specifically are costly to manufacture and have been associated with substantial toxicities in the form of cytokine release syndrome (CRS) and neurotoxicity.[14,56]

CD70 is expressed on many tumor types and the CD70-CD27 signaling axis plays a role in immune evasion, metastasis, and chemoresistance.[57] In non-small cell lung cancer, CD70 upregulation is an early event in the evolution of resistance to traditional chemotherapies and occurs in drug-tolerant persister cells, promoting cell survival and invasiveness.[58] Additionally, mouse models generated using CD70 KO cell lines grown in parallel showed significantly increased survival. This suggests that there is some mechanism upregulating CD70 expression during tumor progression and that this expression promotes tumorigenesis. It has been shown that CD70 expression is increased in recurrent tumors, and CD70 KO resulted in decreased tumorigenicity.[23] As a proof of principle, we confirmed that CD70 expression is more pronounced in higher-grade OSA by assessing a TMA. Interestingly, cell lines that expressed low or no CD70 *in vitro* via flow cytometry showed high levels of CD70 staining in endpoint tumors and lungs when put into mice. In addition to cancer progression, CD70 is minimally expressed in healthy tissues, and expression is restricted to highly activated T, B, and NK lymphocytes and a small subset of dendritic cells.[59] These factors make CD70 a promising TAA target, specifically for later stage OSAs.

Due to this promising link, we designed an scFv-based CD70 CAR to engineer primary NK cells from healthy donors for our preclinical

Figure 5. Treatment with CD70 CAR NK cells results in delayed tumor growth in an orthotopic mouse model of osteosarcoma

(A) Schematic of orthotopic mouse study timeline, including 143B tumor cell implantation into NSG mice (45 mice injected: eight groups, $n = 5$ mice per group; one extra mouse injected per group to account for engraftment failure), treatment, IVIS imaging, caliper measurements, and blood collection. (B) Spaghetti plots showing tumor growth (tumor volume in mm^3) for each individual animal by treatment shown over days post-tumor implantation by treatment group. (C) Kaplan-Meier survival curve of 143B-tumor-bearing mice receiving therapeutic doses. Survival significance was determined by a log rank (Mantel-Cox) test between groups ($n = 5$ mice per treatment group). (D) Peripheral blood was collected weekly and assessed by flow cytometry following RBC lysis; error bars shown are standard deviation between animals in that group on a given collection date ($n = 5$ mice per treatment group). (E) Serum from weekly blood collections was pooled between animals from one treatment group and assessed via IL-15 ELISA ($n = 5$ mice per treatment group). (F) Endpoint tissues (blood, lungs, and tumors) were assessed by flow cytometry for total counts of NK cells (murine $CD45^-$, human $CD45^+$, and human $CD56^+$) and analyzed for statistical significance using ordinary one-way ANOVAs with multiple comparisons ($\alpha = 0.05$, $^*p < 0.05$, $^{**}p < 0.01$, $^{***}p < 0.001$, $^{****}p < 0.0001$). Bar graphs represent the average of animals within that treatment group; error bars show standard deviation ($n = 5$ mice per treatment group). (G) Lungs harvested at endpoint were fixed, paraffin embedded, and stained with CD70. Tissues were analyzed using QuPath and total area of the lung tissue, and area of that tissue composed of metastatic disease was quantified and graphed ($n = 5$ mice per treatment group).

studies. Using the non-viral hyperactive TcBuster transposon system,[42] we were able to deliver a CD70 CAR cassette or multicistronic vector that also armored our NK cells with soluble IL-15 and/or a TGF-β DNR. Interestingly, TGF-β signaling upregulates the expression of CD70.[60] For OSAs, the invasion of bone tissue is known to deregulate bone remodeling, inducing release of cytokines and growth factors normally trapped within the bone matrix, such as TGF-β.[34] When this occurs, there is a positive feedback loop of TGF-β release, signaling, and tumor progression. Furthermore, TGF-β signaling in OSA is shown to promote tumor development and metastatic progression. Simultaneous to transposon engineering, we also knocked out CD70 through CRISPR/Cas9 in primary human peripheral blood NK cells with excellent efficiency and minimal off-targets. Of the 5N off-targets identified for our CD70 sgRNA, none were at biologically relevant sites (J.-W.C., unpublished data) Alongside the minimal off-target CRISPR/Cas9 editing, *TcBuster* has a safer insertion profile than traditional lentiviral engineering,[42,61] and we showed copy-number analysis below the FDA guidelines.

Our *in vitro* testing of the designed constructs uncovered striking differences in effector functions in NK cells; this was especially true with the CAR TR15^{KO} NK cells that had the most pronounced improvements in function. Co-culture luciferase-based killing assays showed CAR TR15^{KO} NK cells are best equipped to eliminate target OSA cell lines. Specifically, against the OSA cell line SaOS-2, we observed potent antitumor activity from CAR TR15^{KO} NK cells. This observation is likely due to the greater expression of CD70 on SaOS-2 cells compared to 143B, as the NK cells lacking CAR yet equipped with IL-15 and TGFβ DNR had a similar antitumor response. Intracellular staining revealed that CD70-CAR-expressing NK cells showed superior cytokine degranulation (CD107, IFN-γ, and TNF-α) against CD70^{high} cell line, SaOS-2. While CAR TR15^{KO} NK cells showed an upward trend in degranulation against 143B, no statistically significant difference was observed. We again suspect this is due to the lower expression of CD70 on 143B cells. At 19.7% CD70^{+}, 143B cells did not induce enough CAR signaling to produce high quantities of cytokine degranulation. Additionally, we found higher background killing of 143B by all NK cell conditions, which could further mask any difference between CD70 CAR expressing and control NK cells. However, this could lend evidence to CD70 CAR NK cells being able to eliminate TAA-negative or low targets. It would be interesting to assess OSA cell line surfacome to determine if certain receptors or ligands can further explain why we observed this phenomenon, as it could lead to additional targets or engineering strategies to further improve CAR NK-cell-based therapies for OSA.

Due to the significant performance of CAR TR15^{KO} NK cells against OSA *in vitro*, we used an orthotopic mouse model of osteosarcoma to assess efficacy against primary tumors and lung (metastatic) lesions. While CAR TR15^{KO} NK cells had a more robust *in vitro* response against the CD70 high cell line, SaOS-2, this cell line is not tumorigenic and was unable to be used for *in vivo* studies. As such, we utilized 143B for these *in vivo* studies, which showed that only CAR TR15^{KO} NK cells had a notable anti-tumor effect, mirroring our *in vitro* data. While the therapeutic cells did not achieve tumor clearance, disease progression was slowed, and there was no evidence of metastatic spread, which is the critical factor determining OSA patient prognosis. This suggests that IL-15 and the TGF-β DNR were critical for CD70 CAR NK cell antitumor activity. CAR TR15^{KO} NK cells had a statistically significant increase in survival compared to PBS control and TR15^{KO}-NK-cell-treated mice. Of the five animals treated with CAR TR15^{KO} NK cells, three showed a decreased tumor growth rate. We found that IL-15 levels remained stable in CAR-TR15^{KO}-NK-cell-treated animals, which was paralleled by NK cell levels seen in the peripheral blood. Lack of persistence is often considered a barrier to successful NK-cell-based therapies; however, our weekly peripheral blood data indicate that IL-15 sustained NK cell persistence *in vivo*. CD70 CAR NK cells also showed greater tissue infiltration, including the primary tumor, compared to other control NK cell conditions. This is critical for immunologically cold tumors, like OSA, particularly in tissues such as the lungs, which are the most common metastatic site. Many cell-based immunotherapies struggle with effector cell homing to the tumor. CAR TR15^{KO} NK cells showed homing not only to the primary tumor but to metastatic lesions as well. nELISA analysis of *in vitro* co-culture killing assays showed increased CXCL9. Tumor expression of CXCL9 and CXCL10 have previously been associated with immune cell recruitment to the tumor site by activated NK cells, suggesting these CAR TR15^{KO} NK cells could promote a secondary, antitumor immune response in addition to direct cytotoxic activity.[62,63] Similarly, nELISA analysis showed an increase in CX3CR1, which regulates NK cell functions, including promoting NK cell migration, activation, and cytotoxic cytokine secretion.[64] In addition to homing to the tumor, CAR TR15^{KO} NK cells persisted in this space for several weeks longer than that was seen in control conditions.

Notably, mice treated with R15^{KO} or CAR R15^{KO} NK cells developed poor haircoat, hunched posture, and significant weight loss (≥25%) within 2 weeks of treatment and were euthanized. As shown in Figures 5D and 5E, these groups exhibited markedly elevated peripheral NK cell counts and serum IL-15 levels early after infusion. Oversecretion of IL-15 has been well documented to induce systemic toxicity in NSG models.[51,52] The addition of other genes within the multicistronic expression cassette (e.g., CAR or TGF-β DNR) appears to reduce IL-15 production and effectively eliminate *in vivo* IL-15-related toxicity, potentially explaining why only the R15^{KO} and CAR R15^{KO} conditions resulted in adverse effects.

There is ongoing work in our group to better understand the mechanisms underlying IL-15-driven toxicity and define the optimal level of IL-15 expression that supports NK cell persistence without adverse effects. While these toxicities are clearly evident in NSG models, which lack functional immune systems, such effects may not fully reflect the clinical context, where immune-mediated regulation and alloreactivity could limit excessive NK cell persistence and cytokine production.

To further mitigate the risk of IL-15 toxicity, several strategies may be considered, including the incorporation of an inducible "off switch" for IL-15 expression, the use of weaker or regulatable promoters, or transient IL-15 delivery through mRNA or circular mRNA. These approaches, discussed in our recent review, could help achieve a balanced level of IL-15 expression that supports persistence while ensuring safety in future translational applications.[65]

While *in vivo* results were promising, we did not see primary tumor clearance by CAR TR15^{KO} NK cells; rather, we saw delayed tumor growth. This may be due to antigen heterogeneity, TME suppression beyond TGF-β, *in vivo* model limitations, or a combination of all these factors. Future studies should focus on assessing additional orthotopic models while mirroring current standards of care (amputation/limb salvage, neo-adjuvant and adjuvant chemotherapy). However, the primary factor affecting OSA patient outcome is the presence of metastatic disease. Interestingly, CAR-TR15^{KO}-NK-cell-treated mice did not show presence of metastatic disease despite surviving longest. Most other treatment conditions were harvested due to primary tumors reaching endpoint before metastatic disease could form. Additionally, CAR-TR15^{KO}-NK-cell-treated mice showed prolonged persistence of therapeutic cells, particularly in circulation and in the lungs. Up to this point, most NK-cell-based therapies have failed due to a lack of persistence in the patient setting. Similarly, cell-based immunotherapies often struggle to home to the tumor site, including sites of metastatic disease; CAR TR15^{KO} NK cells show homing to the primary tumor as well as the lungs. Future studies assessing an OSA model that more closely mirrors patients (e.g., primary tumor excision) would allow for more relevant therapeutic efficacy studies. The use of the new 3D-iOSA model, which recapitulates chromosomal instability as well as metastatic spread when implanted in mice, with the use of primary tumor resection would be relevant.[66] These studies may shed more light on whether CAR TR15^{KO} NK cells hold promise for the OSA patients with the most critical need.

In patients receiving NK-cell-based therapies, one challenge is the potential eradication of these therapeutic cells due to alloreactivity. Alloreactive responses occur when the recipient's immune system recognizes the exogenous NK cells as foreign and mounts an immune response, leading to their rapid destruction. This response is problematic in clinical settings where NK cells from healthy, unrelated donors are used. This results in these NK cells failing to persist and exert their therapeutic effects. To overcome this limitation, future studies should focus on utilizing humanized mice to better mimic human immune responses and evaluate long-term efficacy of NK cell therapies. Humanized and induced pluripotent stem cell (iPSC)-derived NK cell platforms provide standardized, renewable sources of NK cells that can be genetically engineered to improve functionality, persistence, and immune evasion.[67,68] To reduce immune rejection, HLA-E overexpression has been shown to protect engineered cells from NK-mediated lysis by engaging the inhibitory NKG2A receptor.[69] In addition, β2-microglobulin (β2M) knockout with HLA-E rescue has been demonstrated in pluripotent stem cell models to prevent recognition by host CD8$^+$ T cells while maintaining inhibition of alloreactive NK cells.[69] Additionally, multi-dosing strategies, where NK cells are administered in repeated cycles, may help maintain therapeutic populations of NK cells by preventing early elimination and improving their sustained activity *in vivo*. Clinically, repeat-dosing regimens have been incorporated into early-phase NK cell trials to sustain cytotoxic activity, given the limited *in vivo* persistence of transferred cells.[70,71] Moreover, transient lymphodepletion using agents such as fludarabine and cyclophosphamide remains a key conditioning approach to promote NK cell expansion and persistence by temporarily reducing host immune barriers.[72,73] These approaches may provide critical insight into overcoming alloreactivity and enhancing the clinical success of NK-cell-based immunotherapies.

To further assess these engineered NK cells, we performed an nELISA to assess 191 different cytokines and chemokines. At first glance, we determined several significant differences in CAR NK cells co-cultured with SaOS-2 (IL-15, MMP-10, TNF-α, CXCL11, IFN-γ, CCL1, CCL2, CCL7, CX3CL1, CXCL10, CXCL9, GM-CSF, MMP-9, and VEGF-C) and 143B (IL-15). Of these cytokines and chemokines, differences in IL-15 are not surprising, given that some of our engineered NK cells produce soluble IL-15. However, we did not see IL-15 show a statistically significant difference at all E:Ts (nor in both cell lines). This could be explained by NK cells at lower E:T ratios consuming most IL-15 produced due to the more challenging co-culture conditions. Interestingly, we observe more IFN-γ and TNF-α, which are major inflammatory cytokines produced by NK cells. This corresponds with the killing data we see *in vitro*. MMP-9-dependent shedding of ICAM-1 was previously found to augment tumor cell resistance to NK cell killing[74]; this may explain why we see MMP-9 elevated in SaOS-2 samples at the 1:32 ratio. While irrelevant in an *in vitro* co-culture setting, NK cells have been documented to produce GM-CSF, which promotes myeloid cell development and maturation as well as dendritic cell differentiation and survival.[75]

The reason we believe these changes in effector cytokine milieu is important is because OSA is typically classified as an immunologically cold tumor with poor immune infiltration.[76] In the instance where there was successful infiltration into OSA tumors, these engineered NK cells could facilitate the regulation and recruitment of other immune cell types. This was further supported by IPA, which showed that CAR TR15^{KO} NK cells induced upregulation of critical signaling pathways in promoting inflammation and recruitment of other immune cells. Alongside downregulation of tumorigenic signaling pathways, this suggests that our therapy could prime a secondary immune response and serves as an effective frontline therapy that allows for primary tumor targeting and engagement of the host immune response.

In summary, CD70 is a promising target for NK-cell-based therapy for OSA. We designed highly effective transposon constructs and

engineered NK cells efficiently using the non-viral *TcBuster* transposon system. CAR TR15^{KO} NK cells emerged as the most efficacious against OSA, as shown by their potent *in vitro* killing and cytokine production as well as *in vivo* persistence, tumor homing, decreased tumor growth rate, and overall increased survival time. As such, our results support future early-phase clinical testing of CAR TR15^{KO} NK cells in relapsed and refractory OSA patients.

MATERIALS AND METHODS

Antibodies and flow cytometry

Flow cytometry assays were performed on a BD Bioscience LSR Fortessa or a CytoFLEX S flow cytometer (Beckman Coulter). All data were analyzed with FlowJo v.10.4 software (FlowJo LLC). All antibodies, proteins, and dyes used can be found in Table S4. Compensation beads were used to optimize fluorescence for multicolor flow cytometry analysis (BD 552845 CompBeads Anti-Rat and Anti-Hamster Ig k/Negative Control Compensation Particles Set, BD 552843 Anti-Mouse Ig, k/Negative Control Compensation Particles Set, Life Technologies A10346 ArC Amine Reactive Compensation Bead Kit). For cell surface staining, cells were stained with viability and Human or Murine TruStain FcX (BioLegend Fc Receptor Blocking Solution) on ice for 15 min. Subsequent surface marker antibodies in PBS were added and samples incubated on ice for 35 min. For intracellular cytokine staining, osteosarcoma cell lines were plated in a 96-well plate for 24 h to allow cells to re-adhere. NK cells were plated at 2.5E6 cells/mL in NK cell medium without cytokines. After overnight rest, NK cells were added at a 1:1 effector-to-target (E:T) ratio. Brilliant violet anti-CD107a was added to the culture, and cells were incubated for 1 h at 37°C. Brefeldin A and monensin (BD Biosciences, San Jose, CA) were added and cells were incubated for an additional 6 h. Cells were stained with fixable viability dye, then for extracellular antigens. Cells were fixed and permeabilized using BD Cytofix/Cytoperm (BD Biosciences, San Jose, CA) following manufacturer's instructions. Cells were then stained for intracellular IFN-γ and TNF-α and analyzed by flow cytometry.

Cell lines

All osteosarcoma cell lines were purchased and obtained from the American Type Culture Collection (ATCC): 143B (CRL-8303), HOS (CRL-1543), MG-63 (CRL-1427), G-292 (CRL-1423), U2OS (CRL-3455), SJSA-1 (CRL-2098), Raji (CRL-86), K562 (CRL-3344), and SaOS-2 (HTB-85). All cell lines were grown and maintained in accordance with standard cell culture techniques. Both 143B and HOS cells were grown in DMEM. MG-63 was grown in EMEM. U2OS, G-292, and SaOS-2 cells were grown in McCoy's 5A. K562, Raji, and SJSA-1 cells were grown in RPMI-1640. Osteosarcoma cell line media was fortified with 10% fetal bovine serum (FBS) and 1% penicillin/streptomycin. SaOS-2 media was fortified with 20% FBS and 1% penicillin/streptomycin. All cell cultures were incubated in a water-jacketed incubator set at 5% carbon dioxide (CO_2) and at 37°C. All cell lines were authenticated by the ATCC using short tandem repeat profiling. All cell lines were regularly tested and found to be free from mycoplasma. When cell lines were split or harvested for experiments, confluence was at ∼80%.

NK cell isolation

Peripheral blood mononuclear cells (PBMCs) from de-identified healthy human donors were obtained by automated leukapheresis (Memorial Blood Centers, Minneapolis, MN). CD56+CD3− NK cells were isolated from the PBMC population using the EasySep Human NK Cell Isolation Kit (STEMCELL Technologies, Cambridge, MA). NK cells were frozen at 5E6 cells/mL in CryoStor CS10 (STEMCELL Technologies, Cambridge, MA) and thawed into culture as needed. Samples were obtained after informed consent with approval from the University of Minnesota Institutional Review Board (IRB 1602E84302).

NK cell culture and expansion

NK cells were cultured in CTS AIM V SFM supplemented with 5% CTS Immune cell SR (Thermo Fisher Scientific, Waltham, MA), 1% Penicillin/Streptomycin, and IL-2 (200 IU/mL). NK cells were activated by co-culture with X-ray-irradiated (100 Gray) feeder cells (K562 cells expressing membrane-bound IL-21 and 41BB-L) at a 2:1 feeder:NK ratio, both 5 days prior to electroporation and 7 days after electroporation.

CD70 constructs

The CD70 CAR, RQR8, IL-15, TGF-β DNR, and other fragments were synthesized by GenScript and subcloned into the Nanoplasmid with TcBuster transposase sites. All sequences were validated through Sanger sequencing (Eurofins Genomics). Polymerase chain reaction (PCR) was performed using the Q5 High-Fidelity 2X Master Mix and Hi-Fi assembly (NEB).

Design of CRISPR/Cas9 reagents and TIDE analysis

PCR primers were designed to amplify a 400- to 500-bp region surrounding the synthetic guide RNA (sgRNA) target site of CD70 (CD70_Target_01). Genomic DNA was extracted 5 days after electroporation and PCR amplified using AccuPrime Taq DNA Polymerase (Thermo Fisher Scientific, Waltham, MA). For analysis using TIDE, PCR amplicons were sent for Sanger sequencing to Eurofins Genomics, and the resulting Sanger chromatograms were uploaded to the TIDE webtool. Sequences for CD70 sgRNA and PCR primers can be found in Tables S2 and S3, respectively.

Electroporation of activated/expanded NK cells

Day 5 feeder-cell-activated NK cells were washed once with PBS and resuspended at 3.5E6 cells in 50 μL. Protector RNase inhibitor (Sigma Aldrich, St. Louis, MO) was added to the mixture at a concentration of 1 μL per reaction (1:50 dilution) and incubated for 5 min at room temperature, as determined by previous publication.[77] The cell mixture was added to 3 μg of transposase mRNA and 2.5 μg transposon nanoplasmid either alone or with 2.5 μg CD70 sgRNA and 3.75 μg Cas9 mRNA on ice. Transposon nanoplasmid alone was used as a control for all experiments. This mixture was electroporated using the MaxCyte electroporation system (MaxCyte, Rockville, MD) using the Extended T4 setting. NK cells were allowed to recover in the MaxCyte cassette for 30 min at 37°C and were then cultured in 5 mL complete NK cell medium. 2E6 feeder cells were

added (1:1 ratio accounting for cell death post electroporation) for immediate expansion.

Droplet digital polymerase chain reaction

To assess the number of construct copy numbers integrated into genomes, genomic DNA was extracted from cells post-engineering using GeneJET genomic DNA purification columns per manufacturer instructions (Thermo Fisher Scientific). Junction PCR primers with the plasmid backbone subtracted were designed using PrimerQuest software (Integrated DNA Technologies, Coralville IA) using settings for two primers + probe qPCR. Each sample was run as a duplexed assay consisting of a RNaseP internal reference or TcB Junction primer + probe set (HEX) and an MND primer + probe set (FAM). Primers and probes were ordered from IDT. Reactions were set up using the ddPCR Supermix for Probes (no dUTP) (Bio-Rad, Hercules, CA) with 200 ng of genomic DNA per assay according to manufacturer's instructions. Droplets were generated and analyzed using the QX200 Droplet-digital PCR system (Bio-Rad, Hercules, CA). Frequency was calculated as fractional abundance adjusted for two copies of reference sequence per genome using the QuantaSoft v.14.0 software (Bio-Rad, Hercules, CA). Primers and probes can be found in Table S2.

Off-target analysis using polymerase chain reaction

Off-target analysis was performed using one sample from cells treated with CD70 sgRNA ("Sample") and one sample from unedited NK cells ("Control" - NK cells electroporated with non-targeting reagents). Using the predicted off targets as the target amplicons, PCR was performed using 10,000 human genomic copies equivalent by mass, and the primer sets were supplied by Integrated DNA Technologies (Coralville, IA). The PCR was amplified on the Thermo Fisher Scientific QuantStudio5 qPCR system (Waltham, MA). The individual amplicon products were purified and quantified using Quant-iT PicoGreen (Thermo Fisher Scientific, Waltham, MA) and the Bioanalyzer High Sensitivity DNA kit by Agilent (Santa Clara, CA). A total of 59 amplicon primer pairs were prepared for sequencing, including the target site (site "01") and 58 putative off-target sites (sites "02–59"); these primer pairs can be found in Table S3. These libraries were superpooled and sequenced on an Illumina NextSeq. The resulting reads were mapped to the reference amplicon targets, and any indel deviations from the reference sequence were enumerated and calculated as a mutation fraction with a percentage = [# mutant reads for a given indel within the amplicon]/[total # reads for the replicate PCR reaction]. These mutant fractions (MFs) were averaged for the duplicates of samples or controls (to calculate a mean MF), and the means were compared. In cases where only one of two sample or control replicates generated an MF, the mean MF was equal to that value. Schematic of off-target analysis and the percentage of samples edited relative to the control are shown in Figure S1.

IL-15 ELISA

Human IL-15 ELISA kit (Abcam) was used to quantify circulating serum IL-15. Serum was diluted 1:2 before assay with sample diluent provided by the kit.

Histology and immunohistochemistry

Histology was performed at HistoWiz Inc. using a Standard Operating Procedure and fully automated workflow. Where relevant, samples were processed, embedded in paraffin, and sectioned at 4 μm. IHC was performed on Leica Bond RX automated stainer (Leica Microsystems). The slides were dewaxed using xylene and alcohol-based dewaxing solutions. Tris-EDTA-based pH 9 solution for 20 min. The slides were incubated with the rabbit anti-CD70 antibody (Abcam, ab300083) at 1:250 or mouse anti-Mitochondria antibody (Abcam, ab92824) at 1:100 dilution for 30 min. A secondary polymer was used from the Leica Polymer Detection kit to visualize the DAB chromogen. The slides were dried, cover slipped (Tissue-Tek Prisma Coverslipper), and scanned using a Leica Aperio AT2 slide scanner at 40X. For image quantification CD70, QuPath v.0.5.1 was used.[78] Images were uploaded as brightfield (H-DAB) default. A full area of interest was generated for the entirety of the tissue. A thresholder was created with the resolution set to very low, the channel set to DAB, a Gaussian prefilter, smoothing sigma 2, a threshold of 0.20, above threshold classified as positive and below threshold as negative, and region set to everywhere.

Luciferase-based target cell killing assays

Target luciferase expressing osteosarcoma cells (2.5E4 per well) were seeded into a white optically isolated flat-bottom 96-well plate for 24 h to allow cells to re-adhere to the plate. NK cells were thawed from cryopreservation and cultured overnight in medium with 100 IU/mL IL-2. NK cells were added to the wells in triplicate at the indicated E:T ratios. Target cells without effectors served as a negative control (spontaneous cell death) and target cells incubated with 1% Triton X-100 served as a positive control (maximum killing). Co-cultures were incubated at 37°C for 48 h. D-luciferin (potassium salt; Gold Biotechnology, St. Louis, MO) was added to each well at a final concentration of 25 μg/mL and incubated for 5 min with gentle shaking. Luminescence was read in endpoint mode using a BioTek Synergy microplate reader at 4, 24, and 48 h.

nELISA

Cell culture supernatants from luciferase-based killing assays were collected at 48 h. Triplicates were combined in a 96-well v-bottom plate and frozen at −80°C. Samples were shipped on dry ice to Nomic's facilities in Montreal, Quebec, Canada, where they were analyzed using the Maxplex (191 target) and standard protocols. Nomic's protocols are detailed in a preprint publication.[43]

Intraosseous orthotopic osteosarcoma *in vivo* study

All animal procedures were performed in accordance with protocols approved at the University of Minnesota in conjunction with the Institutional Animal Care and Use Committee. To generate orthotopic models, 2.5E5 osteosarcoma cells were injected into the calcaneus of female 6- to 8-week-old immunocompromised (NOD Rag Gamma, Jackson Labs) mice. Tumor volume was calculated via caliper measurements using the formula $V = (W \times W \times L)/2$ where V equals tumor volume, W equals tumor width, and L equals tumor length. To generate i.v. models, 5E5 osteosarcoma cells were injected

i.v. into the tail vein. Mice were anesthetized using 3% isoflurane in 3L oxygen until they no longer responded to toe-pinch. Once anesthesia was induced, ophthalmic ointment was applied, and maintenance dosing of 2% isoflurane was used throughout the rest of the imaging procedure. IVIS Spectrum In Vivo Imaging System was used to acquire the images and ROI with auto exposure, measured in radiance. For tumor imaging, D-luciferin (150 mg/kg, 100 μL volume in PBS) was administered to mice via intraperitoneal (i.p.) injection 5 min prior to image acquisition. ROI boxes were drawn around each mouse. Mice were harvested according to the Mouse Tumor Burden Scoring developed by our lab in conjunction with Research Animal Resources (RAR).

Preparation of NK cells for *in vivo* delivery

Engineered and non-engineered donor NK cells were thawed and injected following 1- to 2-h rest. Cell counts and viability were assessed via trypan blue staining on the Countess 3 system. NK cell concentrations were adjusted to deliver the 5E6 live NK cells via IV injection (100 μL per injection). Matched numbers of non-engineered cells or control NK cells from the same donor were used.

Blood collection

Approximately 100 μL of blood was collected weekly using a 4 to 5 mm lancet from the submandibular vein and a Greiner Bio One MiniCollect Tube K2EDTA. Blood was vortexed and kept on ice until processing in a 96-well plate. For processing, blood was washed with 1X PBS and lysed using ACK lysing buffer for a maximum of three times. Samples were centrifuged at 1,000 × g for 3 min between rounds of washing and lysing.

Tissue dissociation

Immediately following euthanasia, calcaneal tumor fragments (orthotopic model), lungs, and spleens were carefully dissected out using a scalpel. Tissues were cut into small (∼2 mm^3) pieces and added to Miltenyi c-tubes containing 4.7 mL RPMI, 50 μL DNase I (50 mg/mL = 20,000 Kunitz/mL in 1X PBS; Sigma DN25), and 250 μL Collagenase II (20 mg/mL in PBS; Gibco 17101015). Next, we closed the c-tubes tightly, attached them to the GentleMACS Dissociator, and ran the "m_impTumor_02" program. After program termination, c-tubes were detached from the GentleMACS Dissociator and incubated for 50 min at 37°C under continuous rotation using the MACSmix Tube Rotator. Following incubation, c-tubes were again attached to the GentleMACS Dissociator and run using the "m_impTumor_03" program twice. Once finished, cell suspensions were passed through a 70 μm filter into a new 50 mL Falcon tube. Filters were rinsed with 20 mL RPMI, and the resulting suspension was centrifuged for 7 min at 300 × g. After discarding supernatant, red blood cell (RBC) lysis was performed if the pellet had visible red blood cells. Following RBC lysis or if the pellet was clear/opaque, samples were resuspended in 10 mL PBS +1% BSA and counted using the Countess 3 Automated Cell Counter and Trypan Blue.

Ingenuity pathway analysis

Differential analysis of nELISA results were performed with Limma[45] empirical Bayes. Fold changes and *p* values were then used for pathway analysis in QIAGEN IPA (QIAGEN Inc., https://digitalinsights.qiagen.com/IPA).[44] All other analyses and visualizations were performed in R Statistical Software (v.4.1.0; R Core Team 2022).[79]

Statistical analysis

The Student's *t* test was used to evaluate the significance of differences between the two groups. Differences between three or more groups with one data point were evaluated by a one-way ANOVA with multiple comparisons test. Differences between three or more groups with multiple data points were evaluated by a two-way ANOVA with Tukey's multiple comparisons test. Differences between three or more groups with multiple data points were evaluated by the Log rank (Mantel-Cox) test. All assays were repeated in at least two independent donors in triplicate. A Fisher's exact test was used to evaluate immunohistochemistry score tables. The level of significance was set at $\alpha = 0.05$. All statistical analyses were performed using GraphPad Prism 10.

DATA AND CODE AVAILABILITY

All data relevant to the study are included in the article or uploaded as supplemental information.

ACKNOWLEDGMENTS

G.M.R. is supported by the Office of the Director, National Institutes of Health (NIH) under the Award Number F30OD030021. J.G.S. is supported by the T32HL007062-46 Hematology Research Training Program. B.S.M. acknowledges funding from Office of Discovery and Translation, NIH grants R01AI146009, R01AI161017, P01CA254849, P50CA136393, U24OD026641, U54CA232561, P30CA077598, and U54CA268069; Department Of Defense (DOD) grants HT9425-24-1-1005, HT9425-24-1-1002, and HT9425-24-1-0231; and Children's Cancer Research Fund, the Fanconi Anemia Research Fund, and the Randy Shaver Cancer and Community Fund. B.R.W. acknowledges funding from Office of Discovery and Translation, NIH grants R21CA237789, R21AI163731, P01CA254849, P50CA136393, U54CA268069, and R01AI146009; DOD grants HT9425-24-1-1005, HT9425-24-1-1002, and HT9425-24-1-0231; and Children's Cancer Research Fund, the Fanconi Anemia Research Fund, and the Randy Shaver Cancer and Community Fund.

AUTHOR CONTRIBUTIONS

Conceptualization, G.M.R. and J.-W.C. Methodology, G.M.R., J-.W.C., T.J., J.G.S., and B.W.L. Investigation, G.M.R., J.-W.C., J.B.K., Y.Y.V., A.K.G., T.D.F., K.M.F., J.J.P., and E.M.S. Visualization, G.M.R., J.-W.C., T.D.F., T.J., B.W.L. Supervision, G.M.R., J.-W.C., B.R.W., and B.S.M. Writing—original draft, G.M.R. Writing—review and editing, G.M.R., J.G.S., T.D.F., E.P.R., B.R.W., and B.S.M. Guarantor, B.S.M. All authors reviewed and approved the final version.

DECLARATION OF INTERESTS

The authors declare no competing interests.

SUPPLEMENTAL INFORMATION

Supplemental information can be found online at https://doi.org/10.1016/j.omton.2025.201119.

REFERENCES

1. Wu, J., Sun, H., Li, J., Guo, Y., Zhang, K., Lang, C., Zou, C., and Ma, H. (2018). Increased survival of patients aged 0-29 years with osteosarcoma: A period analysis, 1984-2013. Cancer Med. *7*, 3652–3661.

2. Tsuchiya, H., Kanazawa, Y., Abdel-Wanis, M.E., Asada, N., Abe, S., Isu, K., Sugita, T., and Tomita, K. (2002). Effect of timing of pulmonary metastases identification on prognosis of patients with osteosarcoma: the Japanese Musculoskeletal Oncology Group study. J. Clin. Oncol. *20*, 3470–3477.
3. Kager, L., Zoubek, A., Pötschger, U., Kastner, U., Flege, S., Kempf-Bielack, B., Branscheid, D., Kotz, R., Salzer-Kuntschik, M., Winkelmann, W., et al. (2003). Primary metastatic osteosarcoma: presentation and outcome of patients treated on neoadjuvant Cooperative Osteosarcoma Study Group protocols. J. Clin. Oncol. *21*, 2011–2018.
4. Meyers, P.A., Heller, G., Healey, J.H., Huvos, A., Applewhite, A., Sun, M., and LaQuaglia, M. (1993). Osteogenic sarcoma with clinically detectable metastasis at initial presentation. J. Clin. Oncol. *11*, 449–453.
5. Zhu, L., McManus, M.M., and Hughes, D.P.M. (2013). Understanding the Biology of Bone Sarcoma from Early Initiating Events through Late Events in Metastasis and Disease Progression. Front. Oncol. *3*, 230.
6. McNab, W.L. (1979). The "other" venereal diseases: herpes simplex, trichomoniasis and candidiasis. J. Sch. Health *49*, 79–83.
7. Beird, H.C., Bielack, S.S., Flanagan, A.M., Gill, J., Heymann, D., Janeway, K.A., Livingston, J.A., Roberts, R.D., Strauss, S.J., and Gorlick, R. (2022). Osteosarcoma. Nat. Rev. Dis. Primers *8*, 77.
8. Robbins, G.M., Vue, Y.Y., Rahrmann, E.P., and Moriarity, B.S. (2024). Osteosarcoma: A comprehensive review of model systems and experimental therapies. Med. Res. Arch. *12*, 6000. https://doi.org/10.18103/mra.v12i11.6000.
9. Elahi, R., Heidary, A.H., Hadiloo, K., and Esmaeilzadeh, A. (2021). Chimeric Antigen Receptor-Engineered Natural Killer (CAR NK) Cells in Cancer Treatment; Recent Advances and Future Prospects. Stem Cell Rev. Rep. *17*, 2081–2106.
10. Morvan, M.G., and Lanier, L.L. (2016). NK cells and cancer: you can teach innate cells new tricks. Nat. Rev. Cancer *16*, 7–19.
11. Childs, R.W., and Carlsten, M. (2015). Therapeutic approaches to enhance natural killer cell cytotoxicity against cancer: the force awakens. Nat. Rev. Drug Discov. *14*, 487–498.
12. Kim, S.C., Kim, H.J., Park, G.E., Pandey, R.P., Lee, J., Sohng, J.K., and Park, Y.I. (2021). Trilobatin ameliorates bone loss via suppression of osteoclast cell differentiation and bone resorptive function in vitro and in vivo. Life Sci. *270*, 119074.
13. Mailliard, R.B., Son, Y.-I., Redlinger, R., Coates, P.T., Giermasz, A., Morel, P.A., Storkus, W.J., and Kalinski, P. (2003). Dendritic cells mediate NK cell help for Th1 and CTL responses: two-signal requirement for the induction of NK cell helper function. J. Immunol. *171*, 2366–2373.
14. Rafei, H., Daher, M., and Rezvani, K. (2021). Chimeric antigen receptor (CAR) natural killer (NK)-cell therapy: leveraging the power of innate immunity. Br. J. Haematol. *193*, 216–230.
15. Terlikowska, K.M., Dobrzycka, B., and Terlikowski, S.J. (2021). Chimeric Antigen Receptor Design and Efficacy in Ovarian Cancer Treatment. Int. J. Mol. Sci. *22*, 3495. https://doi.org/10.3390/ijms22073495.
16. Park, J.H., Rivière, I., Gonen, M., Wang, X., Sénéchal, B., Curran, K.J., Sauter, C., Wang, Y., Santomasso, B., Mead, E., et al. (2018). Long-Term Follow-up of CD19 CAR Therapy in Acute Lymphoblastic Leukemia. N. Engl. J. Med. *378*, 449–459.
17. Gust, J., Ponce, R., Liles, W.C., Garden, G.A., and Turtle, C.J. (2020). Cytokines in CAR T cell-associated neurotoxicity. Front. Immunol. *11*, 577027.
18. Pfefferle, A., and Huntington, N.D. (2020). You Have Got a Fast CAR: Chimeric Antigen Receptor NK Cells in Cancer Therapy. Cancers *12*, 706. https://doi.org/10.3390/cancers12030706.
19. Ruggeri, L., Mancusi, A., Capanni, M., Urbani, E., Carotti, A., Aloisi, T., Stern, M., Pende, D., Perruccio, K., Burchielli, E., et al. (2007). Donor natural killer cell allorecognition of missing self in haploidentical hematopoietic transplantation for acute myeloid leukemia: challenging its predictive value. Blood *110*, 433–440.
20. Paul, S., and Lal, G. (2017). The Molecular Mechanism of Natural Killer Cells Function and Its Importance in Cancer Immunotherapy. Front. Immunol. *8*, 1124.
21. Al Sayed, M.F., Ruckstuhl, C.A., Hilmenyuk, T., Claus, C., Bourquin, J.-P., Bornhauser, B.C., Radpour, R., Riether, C., and Ochsenbein, A.F. (2017). CD70 reverse signaling enhances NK cell function and immunosurveillance in CD27-expressing B-cell malignancies. Blood *130*, 297–309.
22. Sauer, T., Parikh, K., Sharma, S., Omer, B., Sedloev, D., Chen, Q., Angenendt, L., Schliemann, C., Schmitt, M., Müller-Tidow, C., et al. (2021). CD70-specific CAR T cells have potent activity against acute myeloid leukemia without HSC toxicity. Blood *138*, 318–330.
23. Seyfrid, M., Maich, W.T., Shaikh, V.M., Tatari, N., Upreti, D., Piyasena, D., Subapanditha, M., Savage, N., McKenna, D., Mikolajewicz, N., et al. (2022). CD70 as an actionable immunotherapeutic target in recurrent glioblastoma and its microenvironment. J. Immunother. Cancer *10*, e003289. https://doi.org/10.1136/jitc-2021-003289.
24. Wu, C.-H., Wang, L., Yang, C.-Y., Wen, K.W., Hinds, B., Gill, R., McCormick, F., Moasser, M., Pincus, L., and Ai, W.Z. (2022). Targeting CD70 in cutaneous T-cell lymphoma using an antibody-drug conjugate in patient-derived xenograft models. Blood Adv. *6*, 2290–2302.
25. Jilaveanu, L.B., Sznol, J., Aziz, S.A., Duchen, D., Kluger, H.M., and Camp, R.L. (2012). CD70 expression patterns in renal cell carcinoma. Hum. Pathol. *43*, 1394–1399.
26. Flieswasser, T., Van den Eynde, A., Van Audenaerde, J., De Waele, J., Lardon, F., Riether, C., de Haard, H., Smits, E., Pauwels, P., and Jacobs, J. (2022). The CD70-CD27 axis in oncology: the new kids on the block. J. Exp. Clin. Cancer Res. *41*, 12.
27. O'Neill, R.E., and Cao, X. (2019). Co-stimulatory and co-inhibitory pathways in cancer immunotherapy. Adv. Cancer Res. *143*, 145–194.
28. Chen, Y., Lu, D., Churov, A., and Fu, R. (2020). Research Progress on NK Cell Receptors and Their Signaling Pathways. Mediators Inflamm. *2020*, 6437057.
29. Watzl, C., and Long, E.O. (2010). Signal transduction during activation and inhibition of natural killer cells. Curr. Protoc. Immunol. Chapter *11*. Unit 11.9B.
30. Rav, E., Maegawa, S., Gopalakrishnan, V., and Gordon, N. (2023). Overview of CD70 as a Potential Therapeutic Target for Osteosarcoma. J. Immunol. *211*, 1067–1072.
31. Pahl, J.H., Santos, S.J., Kuijjer, M.L., Boerman, G.H., Sand, L.G., Szuhai, K., Cleton-Jansen, A., Egeler, R.M., Boveé, J.V., Schilham, M.W., and Lankester, A.C. (2015). Expression of the immune regulation antigen CD70 in osteosarcoma. Cancer Cell Int. *15*, 31.
32. Jacobs, J., Deschoolmeester, V., Zwaenepoel, K., Rolfo, C., Silence, K., Rottey, S., Lardon, F., Smits, E., and Pauwels, P. (2015). CD70: An emerging target in cancer immunotherapy. Pharmacol. Ther. *155*, 1–10.
33. Verrecchia, F., and Rédini, F. (2018). Transforming Growth Factor-β Signaling Plays a Pivotal Role in the Interplay Between Osteosarcoma Cells and Their Microenvironment. Front. Oncol. *8*, 133.
34. Lamora, A., Talbot, J., Mullard, M., Brounais-Le Royer, B., Redini, F., and Verrecchia, F. (2016). TGF-β Signaling in Bone Remodeling and Osteosarcoma Progression. J. Clin. Med. *5*, 96. https://doi.org/10.3390/jcm5110096.
35. Hou, A.J., Chang, Z.L., Lorenzini, M.H., Zah, E., and Chen, Y.Y. (2018). TGF-β-responsive CAR-T cells promote anti-tumor immune function. Bioeng. Transl. Med. *3*, 75–86.
36. Philip, B., Kokalaki, E., Mekkaoui, L., Thomas, S., Straathof, K., Flutter, B., Marin, V., Marafioti, T., Chakraverty, R., Linch, D., et al. (2014). A highly compact epitope-based marker/suicide gene for easier and safer T-cell therapy. Blood *124*, 1277–1287.
37. Silvestre, R.N., Eitler, J., de Azevedo, J.T.C., Tirapelle, M.C., Fantacini, D.M.C., de Souza, L.E.B., Swiech, K., Covas, D.T., Calado, R.T., Montero, P.O., et al. (2023). Engineering NK-CAR.19 cells with the IL-15/IL-15Rα complex improved proliferation and anti-tumor effect in vivo. Front. Immunol. *14*, 1226518.
38. Rintz, E., Higuchi, T., Kobayashi, H., Galileo, D.S., Wegrzyn, G., and Tomatsu, S. (2022). Promoter considerations in the design of lentiviral vectors for use in treating lysosomal storage diseases. Mol. Ther. Methods Clin. Dev. *24*, 71–87.
39. Nakamura, K., Nakayama, M., Kawano, M., Ishii, T., Harigae, H., and Ogasawara, K. (2013). NK-cell fratricide: Dynamic crosstalk between NK and cancer cells. OncoImmunology *2*, e26529.
40. Ojo, E.O., Sharma, A.A., Liu, R., Moreton, S., Checkley-Luttge, M.-A., Gupta, K., Lee, G., Lee, D.A., Otegbeye, F., Sekaly, R.-P., et al. (2019). Membrane bound IL-21 based NK cell feeder cells drive robust expansion and metabolic activation of NK cells. Sci. Rep. *9*, 14916.

41. (2024). Guidance for Industry Considerations for the Development of Chimeric Antigen Receptor (CAR) T Cell Products. https://www.fda.gov/media/156896/download.

42. Skeate, J.G., Pomeroy, E.J., Slipek, N.J., Jones, B.J., Wick, B.J., Chang, J.-W., Lahr, W.S., Stelljes, E.M., Patrinostro, X., Barnes, B., et al. (2024). Evolution of the clinical-stage hyperactive TcBuster transposase as a platform for robust non-viral production of adoptive cellular therapies. Mol. Ther. *32*, 1817–1834. https://doi.org/10.1016/j.ymthe.2024.04.024.

43. Dagher, M., Ongo, G., Robichaud, N., Kong, J., Rho, W., Teahulos, I., Tavakoli, A., Bovaird, S., Merjaneh, S., Tan, A., et al. (2025). nELISA: A high-throughput, high-plex platform enables quantitative profiling of the secretome. Preprint at bioRxiv. https://doi.org/10.1101/2023.04.17.535914.

44. Krämer, A., Green, J., Pollard, J., Jr., and Tugendreich, S. (2014). Causal analysis approaches in Ingenuity Pathway Analysis. Bioinformatics *30*, 523–530.

45. Ritchie, M.E., Phipson, B., Wu, D., Hu, Y., Law, C.W., Shi, W., and Smyth, G.K. (2015). limma powers differential expression analyses for RNA-sequencing and microarray studies. Nucleic Acids Res. *43*, e47.

46. Sun, S.-C. (2017). The non-canonical NF-κB pathway in immunity and inflammation. Nat. Rev. Immunol. *17*, 545–558.

47. Ababneh, O., Nishizaki, D., Kato, S., and Kurzrock, R. (2024). Tumor necrosis factor superfamily signaling: life and death in cancer. Cancer Metastasis Rev. *43*, 1137–1163.

48. Leopold Wager, C.M., and Wormley, F.L., Jr. (2014). Classical versus alternative macrophage activation: the Ying and the Yang in host defense against pulmonary fungal infections. Mucosal Immunol. *7*, 1023–1035.

49. Zenobia, C., and Hajishengallis, G. (2015). Basic biology and role of interleukin-17 in immunity and inflammation. Periodontol *69*, 142–159.

50. Jiang, S., Zhou, F., Zhang, Y., Zhou, W., Zhu, L., Zhang, M., Luo, J., Ma, R., Xu, X., Zhu, J., et al. (2020). Identification of tumorigenicity-associated genes in osteosarcoma cell lines based on bioinformatic analysis and experimental validation. J. Cancer *11*, 3623–3633.

51. Wang, M., Krueger, J.B., Gilkey, A.K., Stelljes, E.M., Kluesner, M.G., Pomeroy, E.J., Skeate, J.G., Slipek, N.J., Lahr, W.S., Vázquez, P.N.C., et al. (2024). Precision Enhancement of CAR-NK Cells through Non-Viral Engineering and Highly Multiplexed Base Editing. Preprint at bioRxiv. https://doi.org/10.1101/2024.03.05.582637.

52. Christodoulou, I., Ho, W.J., Marple, A., Ravich, J.W., Tam, A., Rahnama, R., Fearnow, A., Rietberg, C., Yanik, S., Solomou, E.E., et al. (2021). Engineering CAR-NK cells to secrete IL-15 sustains their anti-AML functionality but is associated with systemic toxicities. J. Immunother. Cancer *9*, e003894. https://doi.org/10.1136/jitc-2021-003894.

53. Li, H., Song, W., Li, Z., and Zhang, M. (2022). Preclinical and clinical studies of CAR-NK-cell therapies for malignancies. Front. Immunol. *13*, 992232.

54. Pan, K., Farrukh, H., Chittepu, V.C.S.R., Xu, H., Pan, C.-X., and Zhu, Z. (2022). CAR race to cancer immunotherapy: from CAR T, CAR NK to CAR macrophage therapy. J. Exp. Clin. Cancer Res. *41*, 119.

55. Rodriguez-Garcia, A., Palazon, A., Noguera-Ortega, E., Powell, D.J., Jr., and Guedan, S. (2020). CAR-T Cells Hit the Tumor Microenvironment: Strategies to Overcome Tumor Escape. Front. Immunol. *11*, 1109.

56. Messmer, A.S., Que, Y.-A., Schankin, C., Banz, Y., Bacher, U., Novak, U., and Pabst, T. (2021). CAR T-cell therapy and critical care : A survival guide for medical emergency teams. Wien. Klin. Wochenschr. *133*, 1318–1325.

57. Nolte, M.A., van Olffen, R.W., van Gisbergen, K.P.J.M., and van Lier, R.A.W. (2009). Timing and tuning of CD27-CD70 interactions: the impact of signal strength in setting the balance between adaptive responses and immunopathology. Immunol. Rev. *229*, 216–231.

58. Nilsson, M.B., Yang, Y., Heeke, S., Patel, S.A., Poteete, A., Udagawa, H., Elamin, Y.Y., Moran, C.A., Kashima, Y., Arumugam, T., et al. (2023). CD70 is a therapeutic target upregulated in EMT-associated EGFR tyrosine kinase inhibitor resistance. Cancer Cell *41*, 340–355.e6.

59. Jin, L., Ge, H., Long, Y., Yang, C., Chang, Y.E., Mu, L., Sayour, E.J., De Leon, G., Wang, Q.J., Yang, J.C., et al. (2018). CD70, a novel target of CAR T-cell therapy for gliomas. Neuro Oncol. *20*, 55–65.

60. Yang, Z.-Z., Grote, D.M., Xiu, B., Ziesmer, S.C., Price-Troska, T.L., Hodge, L.S., Yates, D.M., Novak, A.J., and Ansell, S.M. (2014). TGF-β upregulates CD70 expression and induces exhaustion of effector memory T cells in B-cell non-Hodgkin's lymphoma. Leukemia *28*, 1872–1884.

61. Wong, D.P., Roy, N.K., Zhang, K., Anukanth, A., Asthana, A., Shirkey-Son, N.J., Dunmire, S., Jones, B.J., Lahr, W.S., Webber, B.R., et al. (2022). A BAFF ligand-based CAR-T cell targeting three receptors and multiple B cell cancers. Nat. Commun. *13*, 217.

62. Fukuda, Y., Asaoka, T., Eguchi, H., Yokota, Y., Kubo, M., Kinoshita, M., Urakawa, S., Iwagami, Y., Tomimaru, Y., Akita, H., et al. (2020). Endogenous CXCL9 affects prognosis by regulating tumor-infiltrating natural killer cells in intrahepatic cholangiocarcinoma. Cancer Sci. *111*, 323–333.

63. Wennerberg, E., Kremer, V., Childs, R., and Lundqvist, A. (2015). CXCL10-induced migration of adoptively transferred human natural killer cells toward solid tumors causes regression of tumor growth in vivo. Cancer Immunol. Immunother. *64*, 225–235.

64. Bernardini, G., Gismondi, A., and Santoni, A. (2012). Chemokines and NK cells: regulators of development, trafficking and functions. Immunol. Lett. *145*, 39–46.

65. Baughan, S.L., Folsom, T., Johnson, M., Kreuger, J., Webber, B., and Moriarity, B.S. (2025). Perspective: IL-15 Cytokine-Armored NK Cells as Ready-to-Use Immunotherapy for Diverse Malignancies: Therapeutic Potential and Toxicity Risks. Front. Immunol. *16*, 1704404.

66. Bassi, G., Rossi, A., Campodoni, E., Sandri, M., Sarogni, P., Fulle, S., Voliani, V., Panseri, S., and Montesi, M. (2024). 3D tumor-engineered model replicating the osteosarcoma stem cell niche and in vivo tumor complexity. ACS Appl. Mater. Interfaces *16*, 55011–55026. https://doi.org/10.1021/acsami.4c02567.

67. Zhu, H., Blum, R.H., Bernareggi, D., Ask, E.H., Wu, Z., Hoel, H.J., Meng, Z., Wu, C., Guan, K.-L., Malmberg, K.-J., and Kaufman, D.S. (2020). Metabolic Reprograming via Deletion of CISH in Human iPSC-Derived NK Cells Promotes In Vivo Persistence and Enhances Anti-tumor Activity. Cell Stem Cell *27*, 224–237.e6.

68. Lin, X., Sun, Y., Dong, X., Liu, Z., Sugimura, R., and Xie, G. (2023). IPSC-derived CAR-NK cells for cancer immunotherapy. Biomed. Pharmacother. *165*, 115123.

69. Gornalusse, G.G., Hirata, R.K., Funk, S.E., Riolobos, L., Lopes, V.S., Manske, G., Prunkard, D., Colunga, A.G., Hanafi, L.-A., Clegg, D.O., et al. (2017). HLA-E-expressing pluripotent stem cells escape allogeneic responses and lysis by NK cells. Nat. Biotechnol. *35*, 765–772.

70. Ishikawa, T., Okayama, T., Sakamoto, N., Ideno, M., Oka, K., Enoki, T., Mineno, J., Yoshida, N., Katada, K., Kamada, K., et al. (2018). Phase I clinical trial of adoptive transfer of expanded natural killer cells in combination with IgG1 antibody in patients with gastric or colorectal cancer. Int. J. Cancer *142*, 2599–2609.

71. Nahi, H., Chrobok, M., Meinke, S., Gran, C., Marquardt, N., Afram, G., Sutlu, T., Gilljam, M., Stellan, B., Wagner, A.K., et al. (2022). Autologous NK cells as consolidation therapy following stem cell transplantation in multiple myeloma. Cell Rep. Med. *3*, 100508.

72. Williams, S.M., Sumstad, D., Kadidlo, D., Curtsinger, J., Luo, X., Miller, J.S., and McKenna, D.H., Jr. (2018). Clinical-scale production of cGMP compliant CD3/CD19 cell-depleted NK cells in the evolution of NK cell immunotherapy at a single institution. Transfusion *58*, 1458–1467.

73. Ahmadvand, M., Barough, M.S., Barkhordar, M., Faridfar, A., Ghaderi, A., Jalaeikhoo, H., Rajaienejad, M., Majidzadeh, K., Ghavamzadeh, A., and Sarrami-Forooshani, R. (2023). Phase I non-randomized clinical trial of allogeneic natural killer cells infusion in acute myeloid leukemia patients. BMC Cancer *23*, 1090.

74. Fiore, E., Fusco, C., Romero, P., and Stamenkovic, I. (2002). Matrix metalloproteinase 9 (MMP-9/gelatinase B) proteolytically cleaves ICAM-1 and participates in tumor cell resistance to natural killer cell-mediated cytotoxicity. Oncogene *21*, 5213–5223.

75. Louis, C., Souza-Fonseca-Guimaraes, F., Yang, Y., D'Silva, D., Kratina, T., Dagley, L., Hediyeh-Zadeh, S., Rautela, J., Masters, S.L., Davis, M.J., et al. (2020). NK

cell-derived GM-CSF potentiates inflammatory arthritis and is negatively regulated by CIS. J. Exp. Med. *217*, e20191421. https://doi.org/10.1084/jem.20191421.

76. Zhang, Z., Tan, X., Jiang, Z., Wang, H., and Yuan, H. (2022). Immune checkpoint inhibitors in osteosarcoma: A hopeful and challenging future. Front. Pharmacol. *13*, 1031527.

77. Laoharawee, K., Johnson, M.J., Lahr, W.S., Sipe, C.J., Kleinboehl, E., Peterson, J.J., Lonetree, C.-L., Bell, J.B., Slipek, N.J., Crane, A.T., et al. (2022). A Pan-RNase Inhibitor Enabling CRISPR-mRNA Platforms for Engineering of Primary Human Monocytes. Int. J. Mol. Sci. *23*, 9749. https://doi.org/10.3390/ijms23179749.

78. Bankhead, P., Loughrey, M.B., Fernández, J.A., Dombrowski, Y., McArt, D.G., Dunne, P.D., McQuaid, S., Gray, R.T., Murray, L.J., Coleman, H.G., et al. (2017). QuPath: Open source software for digital pathology image analysis. Sci. Rep. *7*, 16878.

79. The R Core Team R. (2025). A Language and Environment for Statistical Computing. https://cran.r-project.org/doc/manuals/r-release/fullrefman.pdf.

OMTON, Volume *34*

Supplemental information

Non-viral TcBuster transposon engineering of CD70-CAR natural killer cells for the treatment of osteosarcoma

Gabrielle M. Robbins, Jae-Woong Chang, Joshua B. Krueger, Young Y. Vue, Alexandria K. Gilkey, Timothy D. Folsom, Tyler Jubenville, Joseph G. Skeate, Benjamin W. Langworthy, Katelyn M. Fitzgerald, Joseph J. Peterson, Erin M. Stelljes, David A. Largaespada, Eric P. Rahrmann, Beau R. Webber, and Branden S. Moriarity

Table S1. NK cell engineering condition breakdown.

Engineering Condition	CD70 KO (Y/N)	RQR8 (Y/N)	IL15 (Y/N)	TGF-β DNR (Y/N)	CAR (Y/N)
Unedited NK Cells	No	No	No	No	No
CD70 KO	Yes	No	No	No	No
$R15^{KO}$	Yes	Yes	Yes	No	No
$TR15^{KO}$	Yes	Yes	Yes	Yes	No
CAR R^{KO}	Yes	Yes	No	No	Yes
CAR $R15^{KO}$	Yes	Yes	Yes	No	Yes
CAR $TR15^{KO}$	Yes	Yes	Yes	Yes	Yes

Table S2. CD70 droplet digital polymerase chain reaction (PCR) primer and probe sequences.

Synthetic Guide RNA (sgRNA) or Primer Name	Sequence
CD70 sgRNA	TCACCAAGCCCGCGACCAAT
MND F Primer	CTGAAATGACCCTGTGCCTTAT
MND R Primer	GCGATCTGACGGTTCACTAAA
MND Probe	/56-FAM/ACCAATCAG/ZEN/TTCGCTTCTCGCTTCT/3IABkFQ/
RNaseP Ex3 F Primer	AGATTTGGACCTGCGAGCG
RNaseP Ex3 R Primer	GAGCGGCTGTCTCCACAAGT
RNaseP Ex3 Probe	/5HEX/TTCTGACCT/ZEN/GAAGGCTCTGCGCG/3IABkFQ/
TcB Junction F Primer	GCGGAACACAGGTTGAAGAACA
TcB Junction R Primer	GGTACCGAGCTCGAATTCAAGG
TcB Junction Probe	/56-FAM/AGAGCTCTA/ZEN/GAGGATTCGACCCATGG/3IABkFQ/

Table S3. CD70 on- and off-target analysis primers sequences.

Amplicon ID	Predicted off-target site Sequence	Locus	Forward Primer for Amplicon	Reverse Primer for Amplicon
CD70_Target_01	TCACCAAGCCCGCGACCAAT	chr19:+6590908	CCATCTCAACTCACCCCAAG	CTGCTTTGGTCCCATTGGT
CD70_OffTarget_02	TCTCCCAGCCCCCGACCATT	chr15:-93693962	TGTAAAAGAGTGGGCAAGTGG	TCCTTCATGGACAAACCTACG
CD70_OffTarget_03	TTGCCAAGCCTGAGACCAAT	chr17:+35343729	AACACACGTTATGCCTGCTT	AAGGTTGATATCCCTACCCAGAA
CD70_OffTarget_04	TCAGCAAGCCCACGGCCATT	chr2:-200382610	ATTCCCCTGGTGGAGTTCTT	TAAGGCAGTCCAACTCAGCA
CD70_OffTarget_05	TCACCAAGCACG-GACCAAT	chr16:-80481970	GAATGTGGGGGCTTATTGGT	GGCTTTACCTAAATAGATTGGCTTT
CD70_OffTarget_06	ACTCCAAGCCCGTGTCCAAT	chr7:+129882447	TGAAATTAAATATTTGGCACTCCA	GGCCTCTTGCAGTCAGTTCT
CD70_OffTarget_07	TCACC-AGCCCGCGGCAAAT	chrX:+65586737	GGCTGCATTTGCAGGACTA	CAGCTCCCATAATGCCTCAG
CD70_OffTarget_08	TCACAGAGCCCCGCGACCAAT	chr1:+221742196	GGGTTGGGCCAATAAGAATC	ATGAGGCCACGCCTTCTTAC
CD70_OffTarget_09	CCACCAAGCCAGCAACCACT	chr8:-28072286	CGGTTTGAGGACTGCCTTAG	TCTTTGCCTCTTCCTCTCCA
CD70_OffTarget_10	GCAGCAAGCCCACGACCCAT	chr3:+49340369	CTCAGGATGGCGCTACACTT	AGGACCACGATAACCTCGAA
CD70_OffTarget_11	TCTCCAAGCCCTCG-CCAAT	chr17:-78344050	GCTCCGGGAAAGACGTTTA	AAAGCCCTGTCTGGTCTTCA
CD70_OffTarget_12	TCACAAAGGCGGCGGCCAAT	chr8:+144331939	GGGTAGGATCGGGAGGAG	AACTTTCGCCCGTCTATGC
CD70_OffTarget_13	CCACCACGCCCGGGGCCAAT	chr19:-47185952	AAGCCCCCAAAATCTGAAAT	ACCTAGGCCTCCCAAAGTG
CD70_OffTarget_14	CCACCAGGCCCGCGCCCAAT	chr17:-4498815	SEQUENCE TOO COMPLEX FOR <200BP PRIMING	
CD70_OffTarget_15	TCACCAAGCCAGCAGCCAGT	chr14:+98648940	TAGCCAACAGCCTACCAACC	TCTCCTGACCCTCTGGAAAG
CD70_OffTarget_16	TCCCCTAGCCCGCAACCAAG	chr8:+97263125	AGGCCATACCATGTTGGG	CTGTTATATTATCCTCCCAGAAAAGC
CD70_OffTarget_17	TCACCAACCCTGCTGCCAAT	chr16:+3739105	ACCCAAAAACCAACCAGTCA	GAGTGGTGCCATTCATCCTT
CD70_OffTarget_18	TCAACAAGCCTGAGAACAAT	chr6:+116483052	GGGATGTGTCAGCAAATGAA	CCCTCAAGTAAAATGGCACAA
CD70_OffTarget_19	TCACCAAGCACGAGGCCAAG	chr17:-2925125	GAGGCAGGAGCTGTTGTTCT	CCTCACGGCCATTATGTCTT
CD70_OffTarget_20	TCACCAAGCCCCTCACCATT	chr11:-120173751	GAACAGTCATCAGATCACACC	CAGCCCTGAGGTCAGTTAGC
CD70_OffTarget_21	TCACAAAGACTGCGACCAAA	chr14:+64565830	GCTCTATGCAAGCCATCCTC	GGCTTCCTCTCCCTGACTCT
CD70_OffTarget_22	TCAGCAAACCCGCGACCTGT	chr17:-79391922	CTTCCCGGTTCTGAAGCTC	GGAGCGTTGCCATACAAGTT
CD70_OffTarget_23	CCACCAAGCCAGCCACCACT	chr2:-237336144	CTGGAGCAGGAAATGAGGAT	AGGCAGCCAAACCAGC
CD70_OffTarget_24	TCACCAATGCAGCCACCAAT	chr18:-30922014	TTCTCAGCCCAGAATTCCAC	ATGGGAGCAGGTGATAGTGC
CD70_OffTarget_25	TCTCCAAGCCCACCACCAAA	chr5:-171239767	TTCTGTAAGTGTGCTACCACC	AGAACTACCAGCCCTGCTGA
CD70_OffTarget_26	TCACCAAGCCAGCAATCAAG	chr6:-2820416	GGAACACAGGCACCTTTCAT	GCCAAACAATTGCTTAATTTATTTTGC
CD70_OffTarget_27	TGATCAAGCCAGCGACCTAT	chr3:+65175634	CCAGACCTCACCACTTACAG	CCACCATTTCTCCTGCTCC
CD70_OffTarget_28	TCACCAAGGCCATGACCAAG	chr13:-25551417	AGATCCTGGTGTTGTTTGGC	TCACCATGAGACCTGTTCCA
CD70_OffTarget_29	CCACCAAGCCCACGCCCACT	chr7:+23194028	CAGCCGGCAGCTCTGAGT	TTGCTGGCCAGCTGG
CD70_OffTarget_30	CCACCAAGCCCACGCCCACT	chr3:-130010700	GCTATGCGTGCTGCTTGC	GGTGCTAAGTCCCTCACTGC
CD70_OffTarget_31	CCACCAAGCCCACGCCCACT	chr1:+1018614	GCTAAGCCCCTCATTGCTC	TTGCGGGCCAGCTGG
CD70_OffTarget_32	TCACCAAGGCCAAGACCACT	chr5:-4531274	CCCTTGCTGACACAGAGGAT	TGTCCCCAGCACAATCACC
CD70_OffTarget_33	CCACCAAGCCCGCACCCACT	chr8:+75178701	GCTCATCCCTCGATCAAGAC	AGCACTCACAGGCCAGCAC
CD70_OffTarget_34	TCACCTACCCGGCCACCAAT	chrX:+152552723	GCTCCCACTTGCAAACAGAG	TACAATTAGGCTGAGAAGC
CD70_OffTarget_35	TCACCAAGCCAGATACCAAG	chr19:-15203126	ACGTGTACAGGCCAGAGG	CCTCCACCCAACCCATTCC
CD70_OffTarget_36	GCACCAAGCCCTCAAGCAAT	chr6:+44109762	CCCACTGGCCAGAGGTCC	AGATGGAACCCTGCTGCTAA
CD70_OffTarget_37	TCACCCAGCCCCCCACCCAT	chr20:-5943370	AGGACAATTGCCATGGGTTT	CCTAGCATGGGGACCTTCTT
CD70_OffTarget_38	TGGCCAGGCCTGCGACCAAT	chr1:-203494073	GGAAAGAGGAGGGGAAACAG	AACTGGGGCTTGGGTTAGAC
CD70_OffTarget_39	CCACCAAGCCCACGCCCAAC	chr6:+27381359	GGGTGCTAAGCCCCTCATT	TGCGCGCGGTGCTTG
CD70_OffTarget_40	TCACCAATCCCGCGCTCAAG	chr19:-56027556	ATCTCCGGGGAACAAAGAAT	ACGCAACCCTTGTGTCTTCT
CD70_OffTarget_41	TCATCAAGCCTGCTACCACT	chr20:-44761604	GGGGATAATGCAGGTGAATG	GGGGAGCTAATAACGGATGC
CD70_OffTarget_42	TTACCAGGCCCTCCACCAAT	chr10:+107340760	GGGTGTCTCAGCTCCAGAAG	CCCTCACCCAATGTGGG
CD70_OffTarget_43	TCACCTAGCACACTACCAAT	chr11:+79831532	TATTGCCGTCACCTAGCACA	AACAAGCAAAAACACACACTGAA
CD70_OffTarget_44	TCACCAAGCCCCTGTCCCAT	chr15:+66143445	CCCTCAGTCTACTCCCTGTCC	TCTGTCTGCACCCGAGAAG
CD70_OffTarget_45	TCACCAAGGCCACAACCAAC	chr16:-57320235	TTGGTTCTGGCTATAACCCCTA	CCAGTAACCCATCACCAAGG
CD70_OffTarget_46	TGAGCAAGCCCACCACCAAT	chr3:-127131521	ATTATCTGCTTGGCTGTCTGC	CACTCCTGACAGGCTCACTG
CD70_OffTarget_47	TCAACAAGCCCAGGACCTAT	chr2:-11562351	GCTTGTTAAGGATGGGTGGA	CAGGGCCTTTCCTCTGCC
CD70_OffTarget_48	CCACCAAGCCGGCGACCACC	chr1:+239925072	AAGCCGGCGACCACCT	GGGAGGTGTAGAGGGAGAGG
CD70_OffTarget_49	CCACCAAGCCCGCGCCCACC	chr10:+80359792	SEQUENCE TOO COMPLEX FOR <200BP PRIMING	
CD70_OffTarget_50	CCACCGAGCCCGCCACCCAT	chr19:+4064714	SEQUENCE TOO COMPLEX FOR <200BP PRIMING	
CD70_OffTarget_51	TCACCAAGACCACCACCACT	chr11:+70787439	SEQUENCE TOO COMPLEX FOR <200BP PRIMING	
CD70_OffTarget_52	TCACCAAGCCCTCAACCTCT	chr3:+142484720	AGGCCCAGACTTGCAACTAA	TCTACCTGGAGACGGTGTCA
CD70_OffTarget_53	TCACCAAGCACTCGCCCAAG	chr2:-96283629	ACGGCACAAAGACAATGACA	GGGCTTCAACATCAGCCATA
CD70_OffTarget_54	TGACCAAGCCTGCTATCAAT	chrX:-30897876	GGCCTCCCTGAAGGAATAGT	TGGACAAATTCCACTGACCA
CD70_OffTarget_55	TCACCAAGCCGTGGACCAAA	chrX:-38484637	TTTTCCCTCTCAGCCTAGCA	GCCTGAGCTTCTCAACATCC
CD70_OffTarget_56	TCACCAAGCCCAGTACCGAT	chrY:-15451805	GTCTCAAGCAGCCCACAATC	TGTAAGTGCCTGCCTCACTG
CD70_OffTarget_57	TCACCGAGCCCGCGACGTAG	chr12:-11171511	CGCATGAACTTCCCGTACTT	GGCCGTTAGCTTAGTCATGG
CD70_OffTarget_58	TCACCAAGCCTGGCACCAGT	chr3:-58646996	CAGGAAAATGCACCCCTCT	GGGGCACCTTTACCTACTCA
CD70_OffTarget_59	TCACCAAGCCCGGCACAAAG	chr2:-24219546	CAGGGAAGAGTCTGGCTGTC	TCCCATCTGCTTACCTCACC

Table S4. Commercially utilized antibodies, proteins, and dyes.

Antibody, Protein, Dye, Bead	Target Species	Clone	Source	Catalogue #
TruStain FcX	Human	N/A	BioLegend	422302
TruStain FcX Plus	Mouse	S17011E	BioLegend	156604
Fixable Viability Dye eFluor 780	N/A	N/A	eBioscience	65-0865-18
PE CD70	Human	113-16	BioLegend	355104
Brilliant violet 605 CD45	Mouse	30-F11	BioLegend	103139
Brilliant violet 421 CD45	Human	2D1	BioLegend	368522
APC CD56 (NCAM)	Human	HCD56	BioLegend	318310
PE/Cyanine7 CD276 (B7H3)	Human	MIH35	BioLegend	135614
PE CD34	Human	QBEND/10	Invitrogen	MA1-10205
Biotinylated CD27 Ligand / CD70 Protein, His, Avitag	Human	N/A	ACRO Biosystems	CDL-H82Q9
APC Streptavidin (High Concentration)	N/A	N/A	Biolegend	405243
eFluor IFNy	Human	4S.B3	Invitrogen	48-7319-42
Brilliant Violet 510 CD107a	Human	H4A3	BioLegend	328632
APC TNF-α	Human	MAb11	BioLegend	502912
Alexa Fluor 700 CD16	Human	3G8	BioLegend	302026
FITC NKG2D	Human	1D11	BioLegend	320820
PE/Dazzle 594 CD69	Human	FN50	BioLegend	310942
PE Lag3	Human	11C3C65	BioLegend	369306
PE/Cyanine7 TIGIT	Human	1G9	BioLegend	142108
Brilliant Violet 510 PD-1	Human	EH12.2H7	BioLegend	329932
Brilliant Violet 421 Tim-3	Human	F38-2E2	BioLegend	345008
Brilliant Violet 605 NKG2A	Human	131411	BD Bioscience	747921
Brilliant Violet 650 NKG2C	Human	134591	BD Bioscience	748165

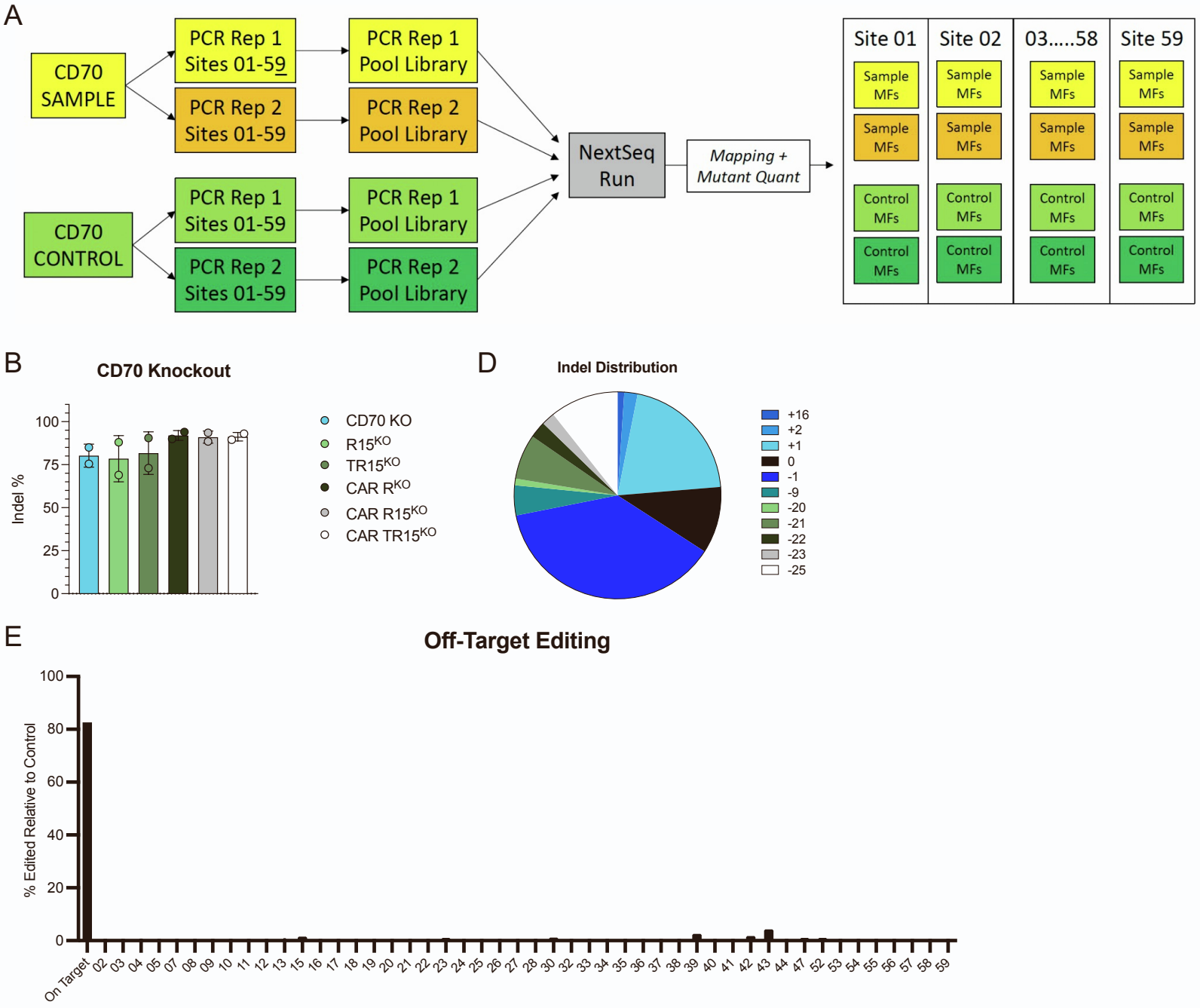

Figure S1. CD70 CRISPR/Cas9 knockout editing efficiency at the genomic level and off-target analysis.

(A) Schematic showing pipeline of off-target analysis. Cells treated with sgRNA ("Sample") and NK cells electroporated with non-targeting reagents ("Control") were assessed. PCRs were performed using the predicted off-target sites as amplicons (59 sites total, including the target site CD70_01). Libraries were super-pooled and sequenced; resulting reads were mapped to the reference genome. **(B)** Bar graph showing CD70 knockout editing efficiency at the genomic level (n = 2 donors). Each point is an average of indel rates for sequencing samples using the forward and reverse primers for each donor (n = 2). Bars represent the average between the two donors with error bars representing standard error of the mean. **(C)** Pie chart showing the frequency of each insertion or deletion detected in the samples from both donors (n = 2). **(E)** Top 58 predicted off-target sites and their editing rates as assessed by PCR and NGS (n = 1 donor; 2 technical replicates)

A

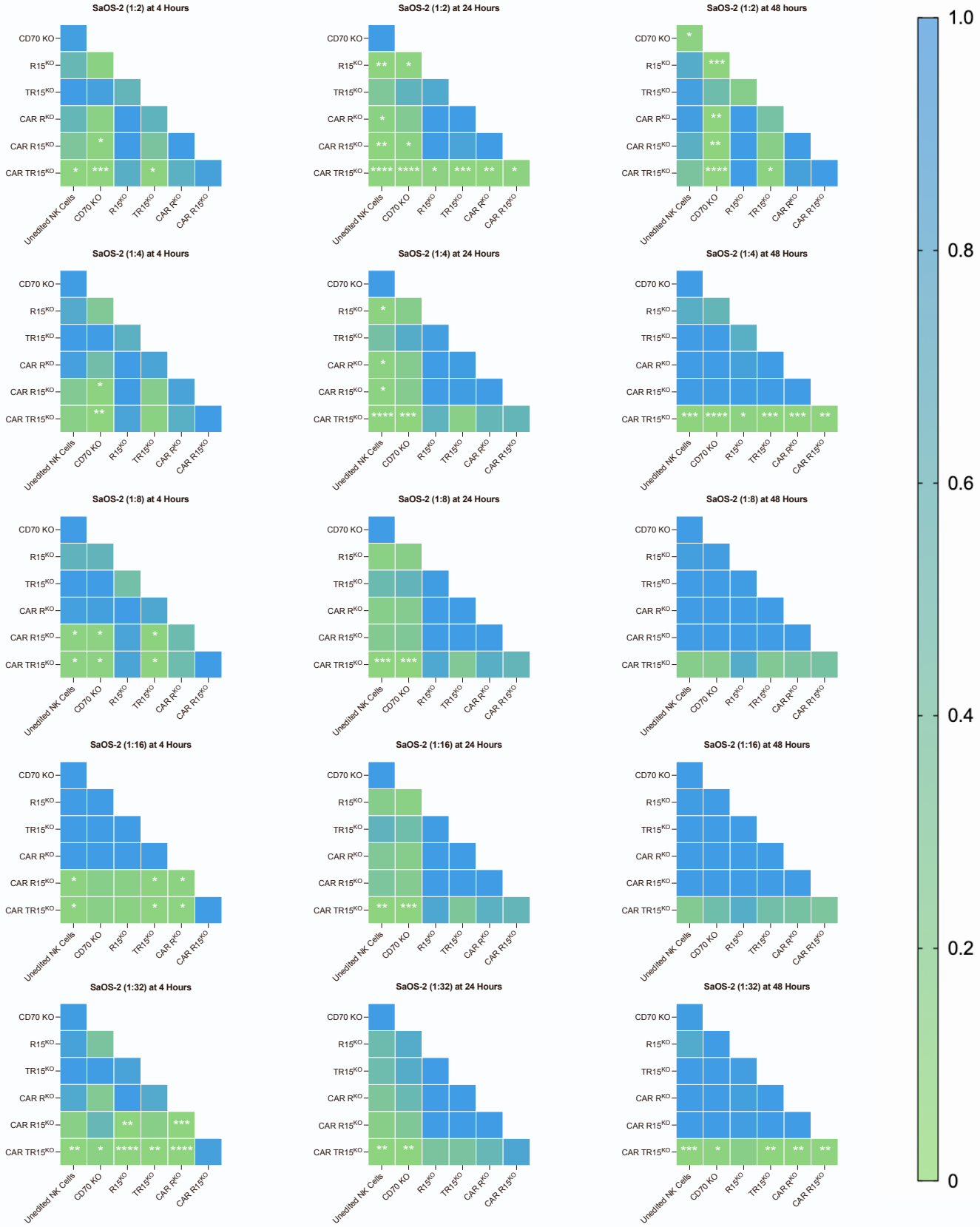

Figure S2. SaOS-2 co-culture luciferase-based killing assays multiple comparisons.

(A) Co-culture experiments were analyzed using two-way ANOVAs with Tukey's multiple comparisons tests. P-values from the Tukey's multiple comparisons were used to generate heat maps in GraphPad Prism 10. Heat maps for co-cultures against SaOS-2 for each time point and effector-to-target ratio are shown (*p<0.05, **p<0.01, ***p<0.001, ****p<0.0001).

A

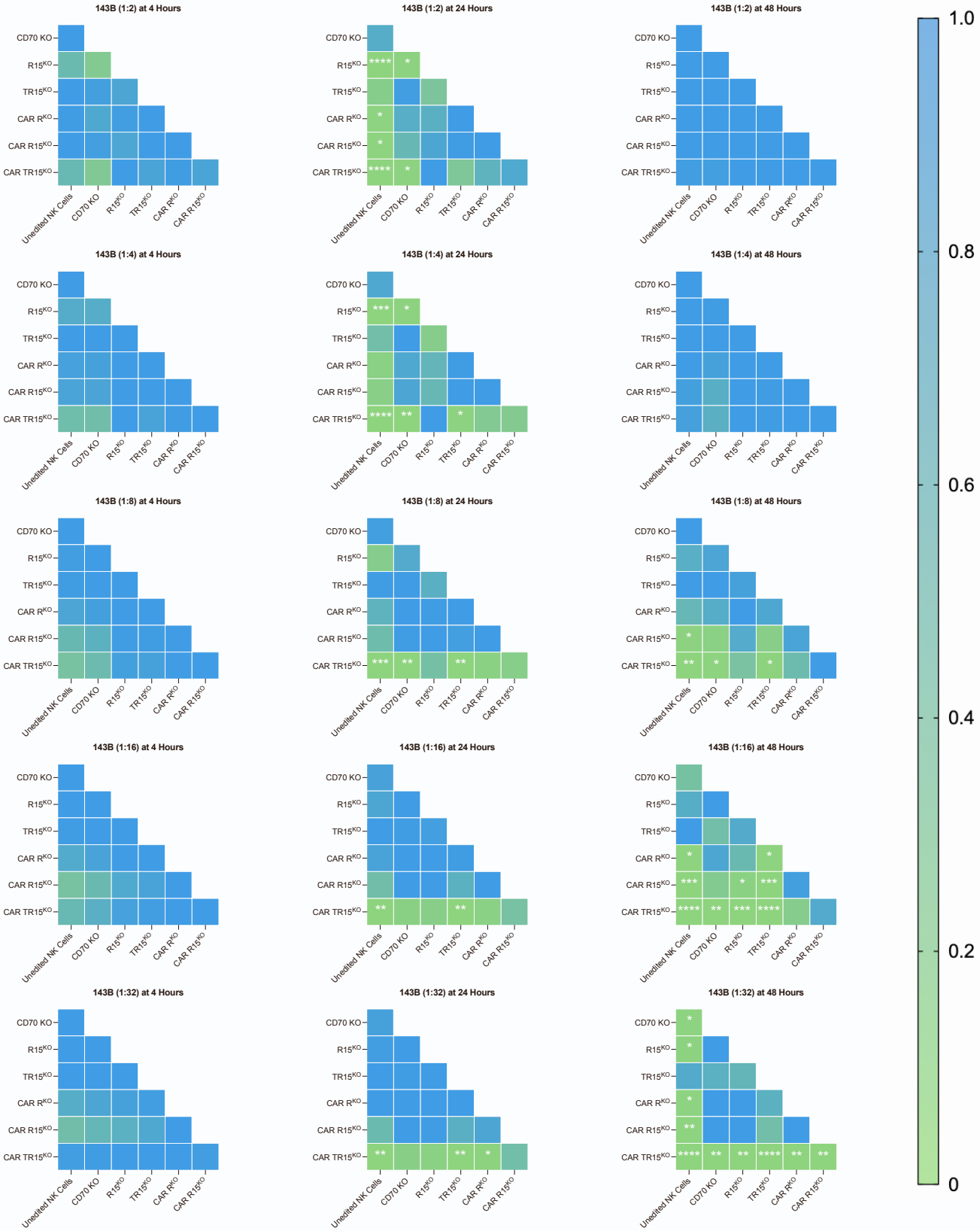

Figure S3. 143B co-culture luciferase-based killing assays multiple comparisons.

(A) Co-culture experiments were analyzed using two-way ANOVAs with Tukey's multiple comparisons tests. P-values from the Tukey's multiple comparisons were used to generate heat maps in GraphPad Prism 10. Heat maps for co-cultures against 143B for each time point and effector-to-target ratio are shown (*p<0.05, **p<0.01, ***p<0.001, ****p<0.0001).

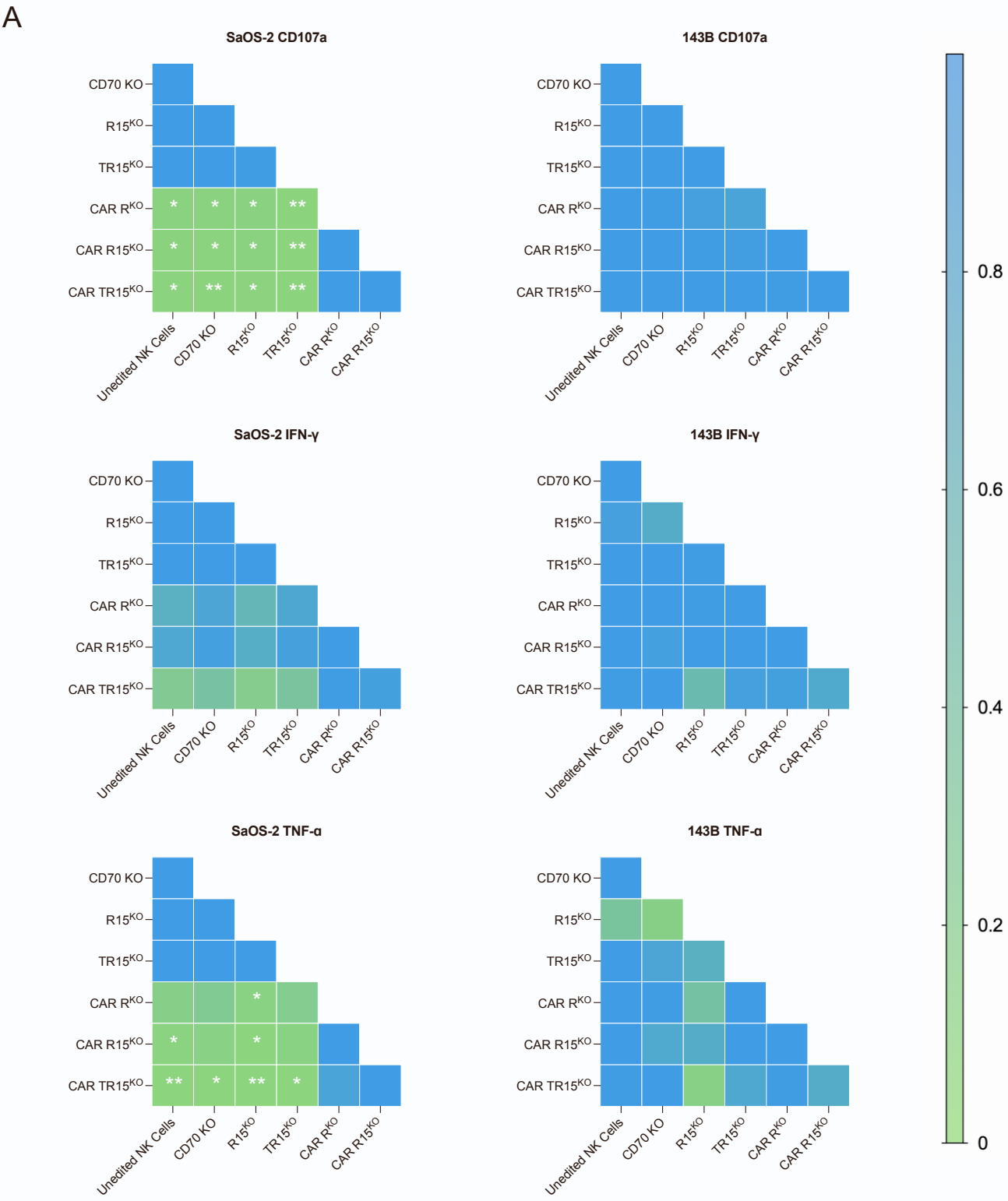

Figure S4. Co-culture intracellular cytokine staining assays multiple comparisons.

(A) Engineered NK cells from 1:1 effector-to-target ratio co-cultures with OS target cells were assessed using intracellular cytokine staining. These results were analyzed using two-way ANOVAs with Tukey's multiple comparisons tests. P-values from the Tukey's multiple comparisons were used to generate heat maps in GraphPad Prism 10. Heat maps for the three different intracellular cytokine stains (CD107a, IFN-γ, and TNF-α) are shown (*p<0.05, **p<0.01, ***p<0.001, ****p<0.0001).

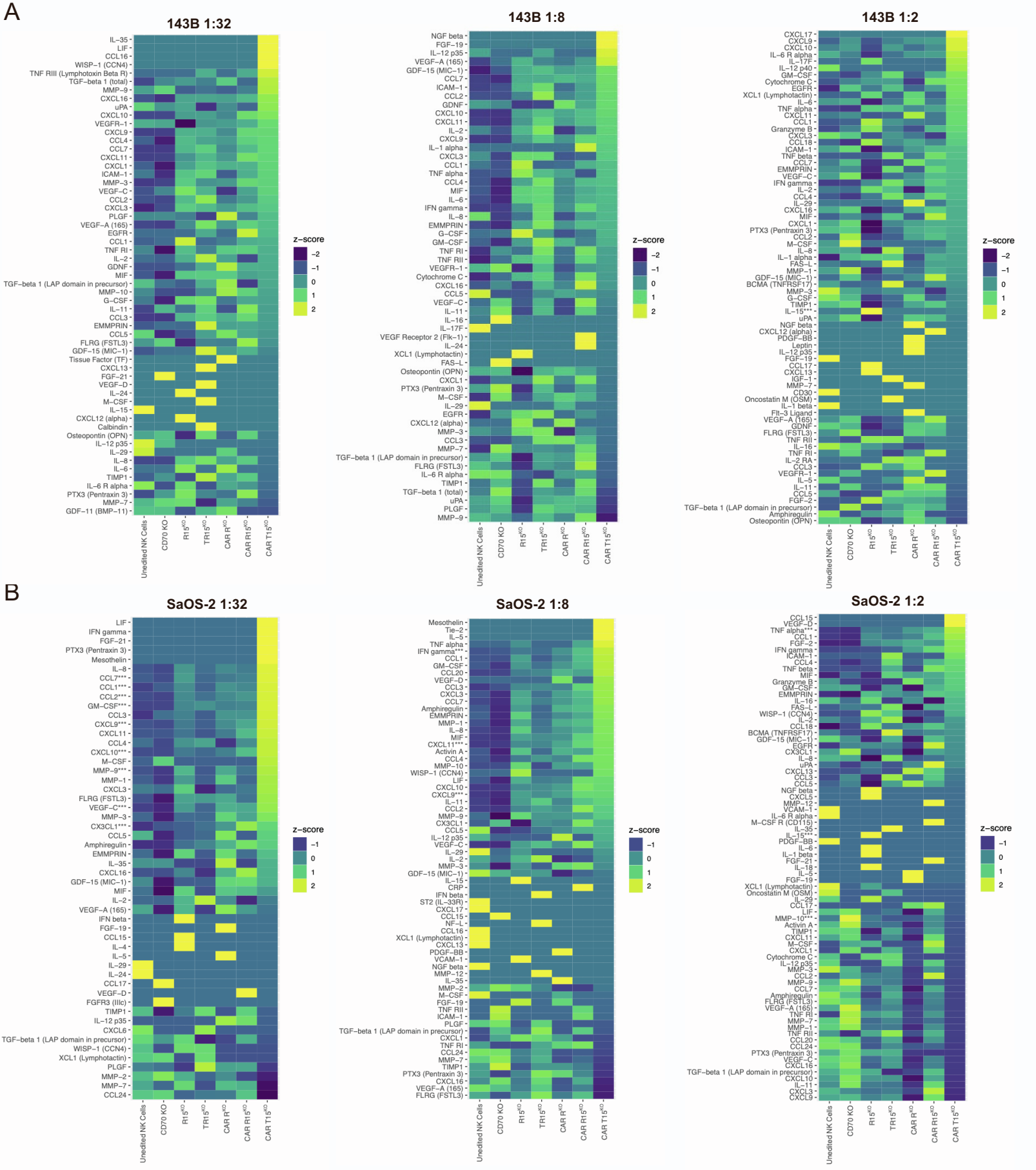

Figure S5. Z-score heat maps from co-culture cytokine and chemokine activity.

(A-B) Heat maps showing z-scores of cytokines and chemokines in co-culture experiments of engineered NK cells against OS target cells, 143B **(A)** and SaOS-2 **(B)** at indicated effector-to-target ratios.

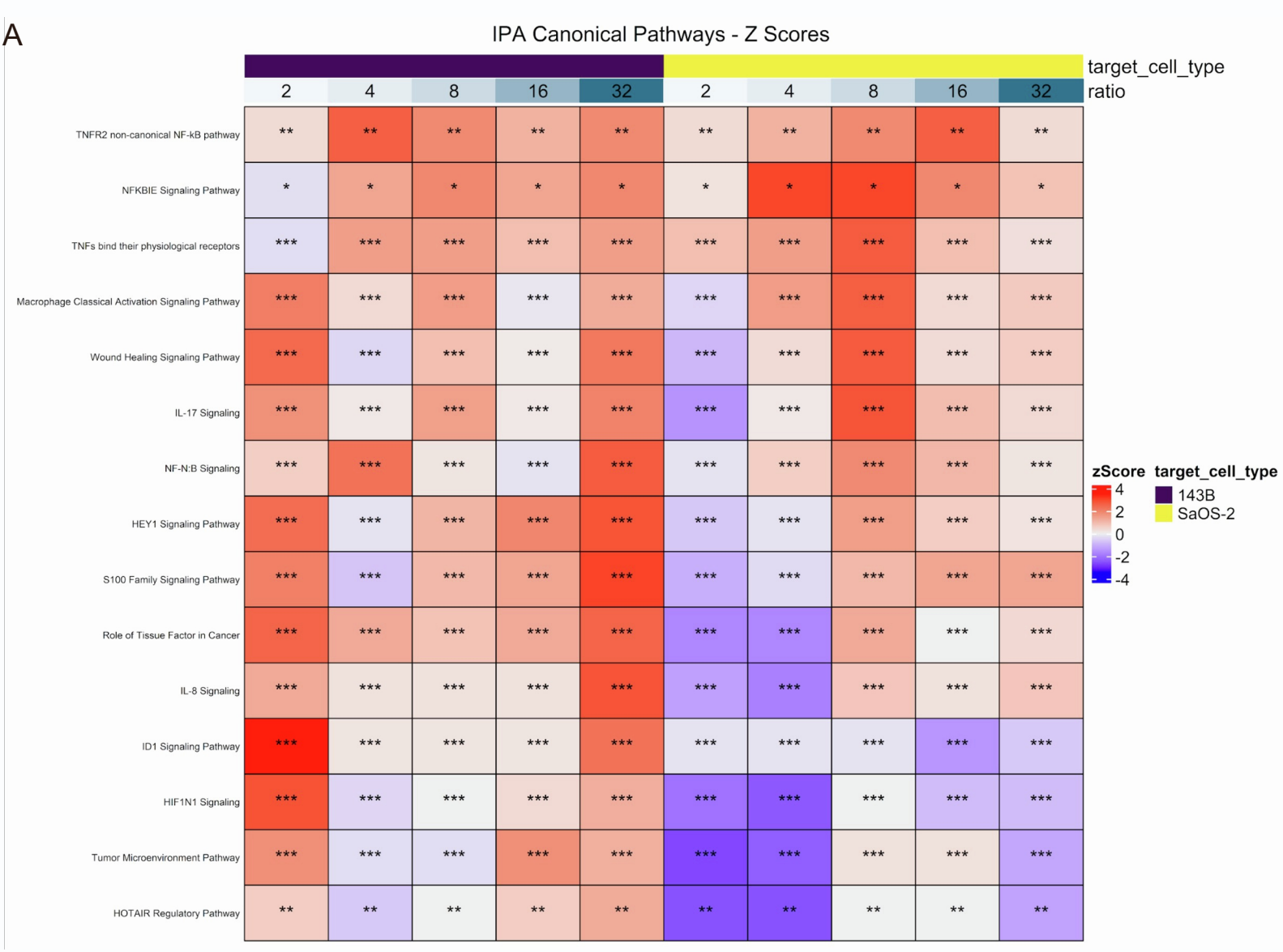

Figure S6. Heat map of ingenuity pathway analysis (IPA) canonical pathways for nELISA data.

(A) nELISA cytokine and chemokine data was run through IPA comparing CAR TR15^{KO} NK cells to unedited NK cells co-cultured with OS cell lines 143B or SaOS-2. Effector to target ratios assessed include 1:2, 1:4, 1:8, 1:16, and 1:32 and are represented by the number of target cells shown above the heat map. IPA results in the form of a heat map of canonical pathways are shown with upregulated pathways in red and downregulated pathways in blue (*p<0.05, **p<0.01, ***p<0.001, ****p<0.0001).

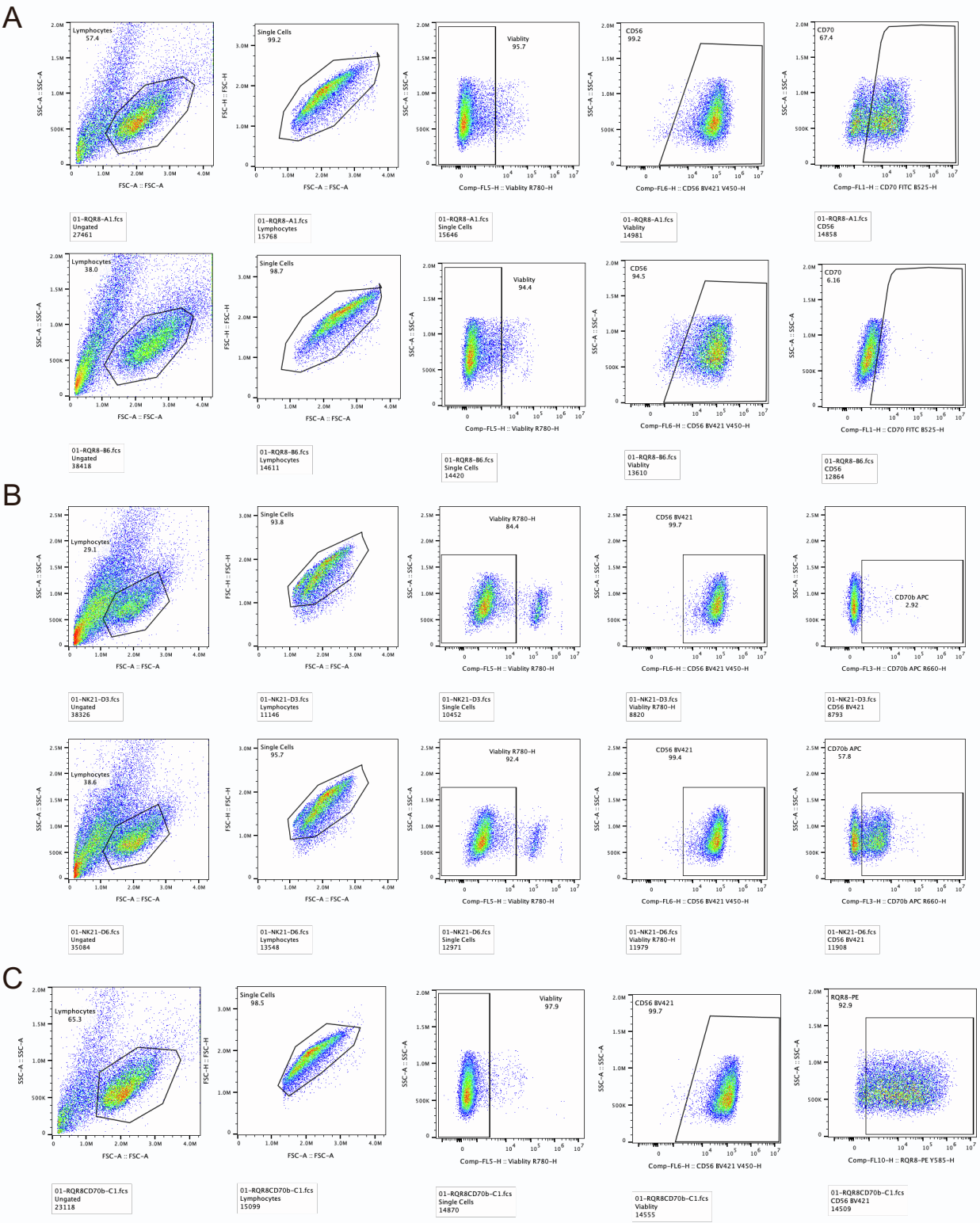

Figure S7. Engineered NK cell flow cytometry gating strategy.

(A) FSC vs SSC dot plots of representative gating strategy analyzing CD70 expression. A healthy donor (upper panels) and the same donor with a CD70 KO (lower panels) are shown. **(B)** FSC vs SSC dot plots of representative gating strategy analyzing CD70 protein expression. A healthy donor (upper panels) and the same donor with a CD70 CAR (lower panels) are shown. **(C)** FSC vs SSC dot plots of representative gating strategy analyzing RQR8 expression. A healthy donor (upper panels) and the same donor with a CD70 KO (lower panels) are shown.

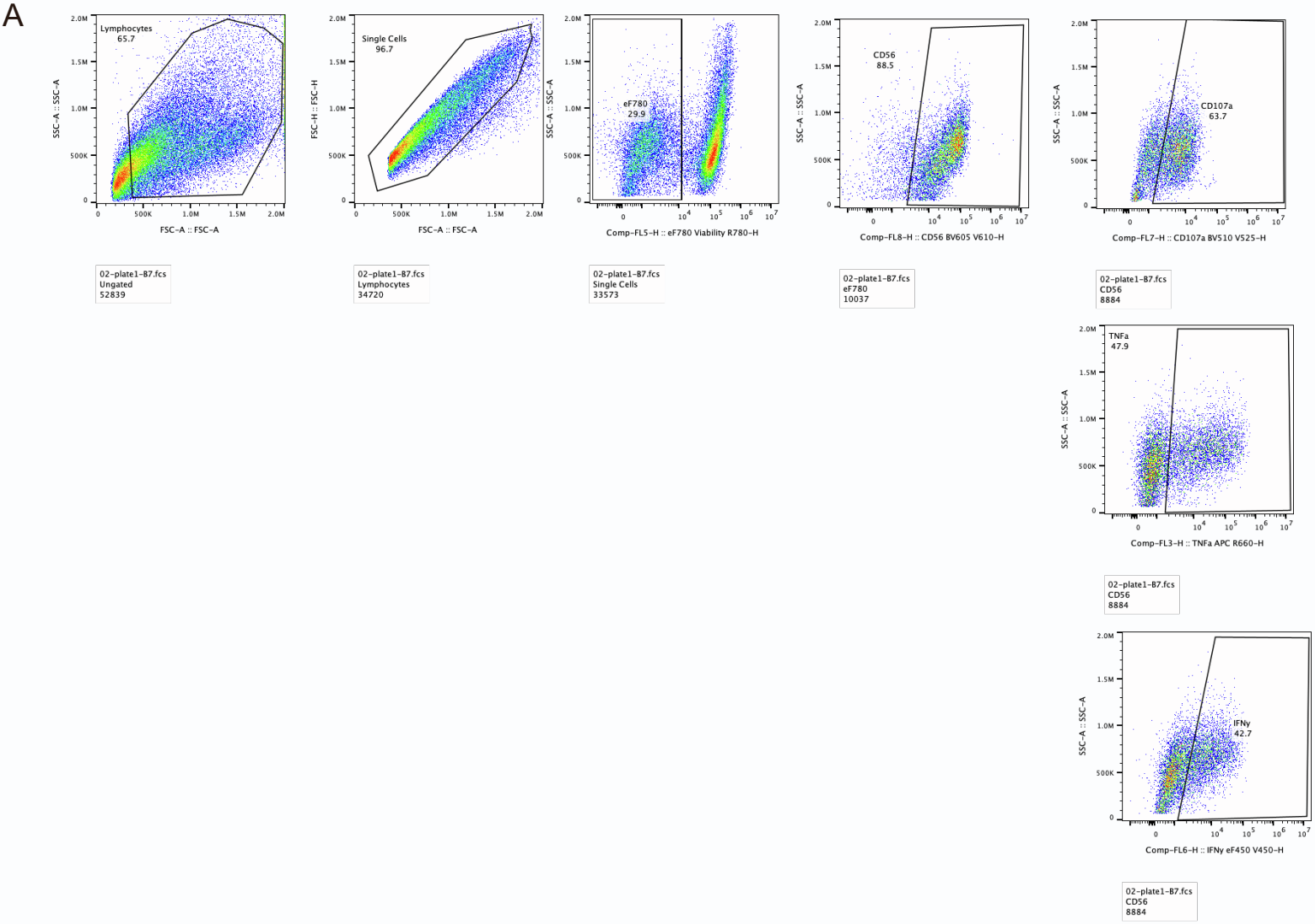

Figure S8. NK cell intracellular staining flow cytometry gating strategy.

(A) FSC vs SSC dot plots of representative gating strategy analyzing CD107a (top), TNF-α (middle), and IFN-γ (bottom).

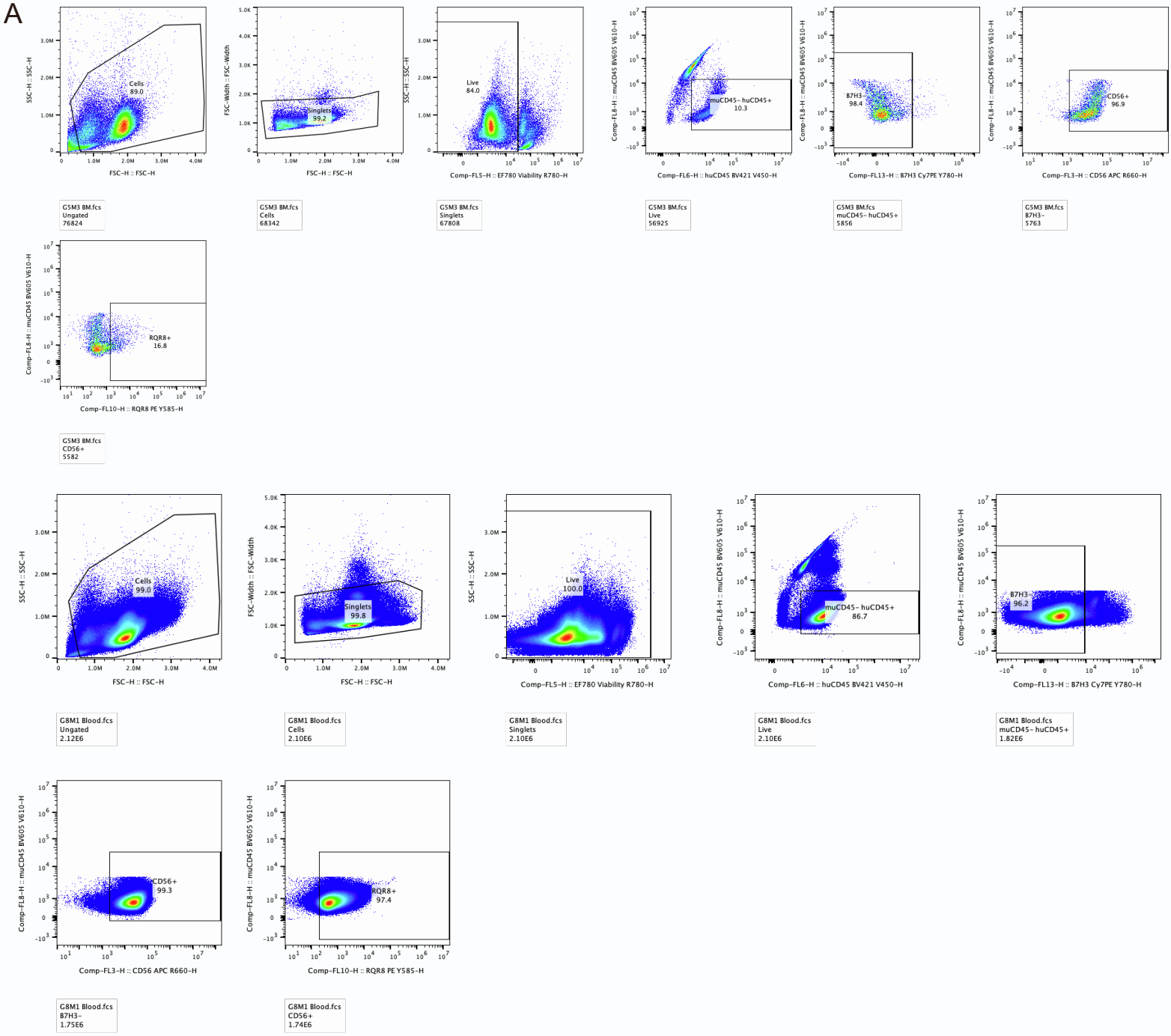

Figure S9. Orthotopic *in vivo* study flow cytometry gating strategy.

(A) FSC vs SSC dot plots of representative gating strategy analyzing RQR8 expression. Blood from mice treated with TR15^{KO} NK cells (upper panels) and mice treated with CAR TR15^{KO} NK cells (lower panels) are shown.